WT-1118 (EX)
EXTRACTED VERSION

OPERATION TEAPOT

Project 2.4. Gamma Dose Rate Versus Time and Distance

February-May 1955

Nevada Test Site

NOTICE

This is an extract of WT-1118, Operation TEAPOT, which remains classified CONFIDENTIAL/RESTRICTED DATA as of this date.

Extract version prepared for:

Director
DEFENSE NUCLEAR AGENCY
Washington, D.C. 20305

1 January 1981

~~UNCLASSIFIED~~
SECURITY CLASSIFICATION OF THIS PAGE (When Data Entered)

REPORT DOCUMENTATION PAGE	READ INSTRUCTIONS BEFORE COMPLETING FORM
1. REPORT NUMBER: WT-1118 (EX) ✓	2. GOVT ACCESSION NO.: AD-A995096
3. RECIPIENT'S CATALOG NUMBER:	
4. TITLE (and Subtitle): Operation TEAPOT ● Project 2.4 ● Gamma Dose Rate Versus Time and Distance	5. TYPE OF REPORT & PERIOD COVERED: 18 D.t.
6. PERFORMING ORG. REPORT NUMBER: WT-1118 (EX)	
7. AUTHOR(s): J. B. Graham	8. CONTRACT OR GRANT NUMBER(s): 12 55
9. PERFORMING ORGANIZATION NAME AND ADDRESS: Headquarters Field Command, Defense Atomic Support Agency, Sanida Base, Albuquerque, New Mexico	10. PROGRAM ELEMENT, PROJECT, TASK AREA & WORK UNIT NUMBERS: 11 Jan. 61
11. CONTROLLING OFFICE NAME AND ADDRESS: 12 DNA 01-79-C-0455.	12. REPORT DATE: October 28, 1959
	13. NUMBER OF PAGES: 59
14. MONITORING AGENCY NAME & ADDRESS (if different from Controlling Office)	15. SECURITY CLASS. (of this report): Unclassified
	15a. DECLASSIFICATION/DOWNGRADING SCHEDULE

16. DISTRIBUTION STATEMENT (of this Report)

Approved for public release; unlimited distribution.

17. DISTRIBUTION STATEMENT (of the abstract entered in Block 20, if different from Report)

18. SUPPLEMENTARY NOTES

This report has had the classified information removed and has been republished in unclassified form for public release. This work was performed by the General Electric Company-TEMPO under contract DNA001-79-C-0455 with the close cooperation of the Classification Management Division of the Defense Nuclear Agency.

19. KEY WORDS (Continue on reverse side if necessary and identify by block number)

Operation TEAPOT
Gamma Dose Rate

20. ABSTRACT (Continue on reverse side if necessary and identify by block number)

346420

DD FORM 1 JAN 73 1473 EDITION OF 1 NOV 65 IS OBSOLETE

Unclassified

* Per: telecon w/Betty Fox, Chief, DNA Tech Libr'y.
Div.: the Classifed References contained herein may remain. 5 Sept.'79
Vic LaChance
DDA-2

**Verified for Extracted Versions.
9 July'80
pfcooper, DTIC/DDA-2

FOREWORD

This report has had classified material removed in order to make the information available on an unclassified, open publication basis, to any interested parties. This effort to declassify this report has been accomplished specifically to support the Department of Defense Nuclear Test Personnel Review (NTPR) Program. The objective is to facilitate studies of the low levels of radiation received by some individuals during the atmospheric nuclear test program by making as much information as possible available to all interested parties.

The material which has been deleted is all currently classified as Restricted Data or Formerly Restricted Data under the provision of the Atomic Energy Act of 1954, (as amended) or is National Security Information.

This report has been reproduced directly from available copies of the original material. The locations from which material has been deleted is generally obvious by the spacings and "holes" in the text. Thus the context of the material deleted is identified to assist the reader in the determination of whether the deleted information is germane to his study.

It is the belief of the individuals who have participated in preparing this report by deleting the classified material and of the Defense Nuclear Agency that the report accurately portrays the contents of the original and that the deleted material is of little or no significance to studies into the amounts or types of radiation received by any individuals during the atmospheric nuclear test program.

Pages 1 thru 3 deleted

ABSTRACT

Project 2.4 objectives were: (1) to measure the gamma intensity versus time of an underground nuclear detonation at several distances from ground zero; and (2) to measure the neutron-induced gamma activity versus time in the vicinity of ground zero of air bursts and to determine the decay rate of this activity. The project participated in five shots.

Gamma-dose-rate measurements were made downwind and upwind from ground zero following Shot Ess. Shot Ess was detonated 67 feet underground and had a yield of 1.2 kt. Gamma measurements were made at ranges from 300 to 6,100 yards along azimuths of 80 degrees and 120 degrees and at ranges of 700 and 1,650 yards for azimuths of 220 degrees and 280 degrees. Following air bursts Wasp and Wasp', which were detonated at altitudes of 762 and 740 feet with yields of 1.2 and 3.1 kt respectively, gamma dose rates were measured as follows:

	Range, yd	Azimuth, degrees
Wasp	437	197
	642	95
Wasp'	470	338
	517	211
	517	98

Two main types of instruments were used: scintillation detectors, for measuring high gamma-radiation rates; and ion-chamber detectors, for measuring both high and low gamma-radiation rates. An experimental cadmium-sulfide (CdS) detector was used with the regular instruments to check its behavior under field conditions. The repeatability of this type of detector was not good enough to consider it for future instrumentation. A detector in a beach ball dropped into Shot Ess crater could not be recovered.

Dose-rate-versus-time data from the underground event supported a power-law decay with a slope of -1.2 after 10 minutes. At times earlier than 10 minutes, the dose-rate records reflected the arrival and passage of the air-borne radioactive debris at the detector stations and, thus, did not lend themselves to dose-rate decay analysis.

The dose-rate-versus-time data from the air bursts, Wasp and Wasp', showed radiation emanations from isotopes in the soil. Al^{28}, Mn^{56}, and Na^{24} were the chief contributors. An attempt was made to correlate results of Shots Wasp and Wasp' with Shots Moth and Tesla, but instrument failure made this correlation impossible.

FOREWORD

This report presents the final results of one of the 56 projects comprising the Military Effects Program of Operation Teapot, which included 14 test detonations at the Nevada Test Site in 1955.

For overall Teapot military-effects information, the reader is referred to "Summary Report of the Technical Director, Military Effects Program," WT-1153, which includes the following: (1) a description of each detonation including yield, zero-point environment, type of device, ambient atmospheric conditions, etc.; (2) a discussion of project results; (3) a summary of the objectives and results of each project; and (4) a listing of project reports for the Military Effects Program.

CONTENTS

TABLES

FIGURES

Chapter I
INTRODUCTION

1.1 OBJECTIVES

Project 2.4 had two objectives: (1) to measure the gamma intensity versus time of a subsurface nuclear detonation at several distances from ground zero; and (2) to measure the neutron-induced gamma activity versus time in the vicinity of ground zero of air bursts and determine the decay rate of this activity.

1.2 BACKGROUND

1.2.1 Underground Burst. Prior to Operation Jangle, the only possible basis for residual radiation predictions was Shot Baker, Operation Crossroads, although it was realized that explosions underground might be quite different (Reference 1). Collection of additional experimental data on the gamma dose rate versus time at various distances from an underground detonation was considered important for the prediction of gamma doses from such detonations. This specific task was given to Project 2.4 of Operation Teapot.

1.2.2 Neutron-Induced Activity. Prior to Operation Teapot only a limited amount of information had been obtained relative to neutron-induced residual gamma fields. Furthermore, the Teapot air-burst events presented an excellent opportunity to measure neutron-induced gamma intensities and decay rates without complications from fission-product activity. The results of the Operation Teapot measurements could be compared with predictions based on information published in "The Capabilities of Atomic Weapons," TM 23-200 (Reference 2), to check the accuracy of these predictions.

1.3 THEORY

1.3.1 Underground Residual Activity. The results of Operation Jangle investigations indicated that the residual activity from underground bursts was fission-product fallout (Reference 3). This fallout was deposited in the form of fine glassy particles, about 200 microns in diameter, on top of earth previously deposited by the base surge. The residual activity from underground bursts was therefore the same as that of surface bursts, except for distribution and magnitude.

Experimentally, it was found that the gamma dose rate from a mixture of fission products followed a $t^{-1.2}$ law of decay with time (Reference 4). The indications are that this law gives a fair approximation to gamma dose rate for times as early as 10 seconds and extending over periods of many days. (See Reference 5 and additional references given there.)

Thus, the dose rate at any time after a few seconds may be written

$$I = I_1 t^{-1.2} \qquad (1.1)$$

Where I_1 = dose rate at unit time, usually chosen as one hour.

1.3.2 Neutron-Induced Residual Activity. When a nuclear detonation occurs high enough above the surface so that no appreciable amount of dust or soil particles are carried into the radioactive cloud, the only residual activity possible is that induced in the soil. Without the scavenging effect of dust, the fission products from the detonation remain suspended in the atmosphere for a long time and gradually diffuse through a sufficiently large volume (the total atmosphere of the earth) and become nonhazardous from a military standpoint.

Both gamma rays and neutrons have sufficient range in air to reach the surface and activate the elements of the soil. However, because the cross section for gamma-induced nuclear reactions is so much smaller than that for neutrons, the activity induced by gamma flux may be neglected (Reference 6).

It can therefore be safely assumed that the residual contamination in the vicinity of an air burst is mainly produced by the bombardment of soil elements by neutrons. Neutron flux produced by thermal fission has been shown to have an energy distribution known as a Watt Spectrum (Reference 7). The neutron energy distribution from a nuclear device, on the other hand, will depend on the construction as well as the design of the device itself. Hanscome and Willet (Reference 8) made neutron measurements during Operation Teapot (Project 2.2) and give a more detailed account of neutron fluxes and spectra. Farther than 300 yards from the device used, the neutron spectrum remains essentially the same with distance. Furthermore, most of the activation will be produced by slow neutrons (References 9 and 10), since the absorption cross sections are generally greatest in this region. Cowan and Cook, using soil analysis given in Reference 11, computed the relative importance factor for elements found in Nevada soil in contributing to the residual gamma activity. The following expression was used for this computation:

$$F_2 = \frac{\sigma_1 N_1 f_2}{T_2} e^{-0.693\, t/T_2} \qquad (1.2)$$

Where: Subscript 1 refers to parent isotope
Subscript 2 refers to daughter isotope
σ = cross section, barns/atom (for thermal neutrons)[1]
N = number of atoms of parent isotope per cm^3 of soil
f = factor to account for energy dependence of dose rate versus disintegration rate
T_2 = half life of daughter isotope, hours
t = time after burst, hours

From the above expression and the above-mentioned analysis of Nevada soil, the four most important isotopes contributing to the gamma activity in early times (0 to 20 hours) after an air burst in order of their importance should be Na^{24}, Mn^{56}, K^{42}, and Fe^{59} (Table 3.8).

[1] The assumption that most of the activation is produced by thermal neutrons has been borne out by measurements (Reference 12).

Chapter 2
PROCEDURE

2.1 OPERATIONS

In order to achieve the primary objective of Project 2.4 (to measure the gamma-radiation dose rate versus time as a function of distance for the underground event), station locations were chosen to provide maximum information on the downwind portion of the fallout pattern. Based on a predicted surface wind from 285 ± 20 degrees, two main instrument lines were set up on azimuths of 80 and 120 degrees to cover the main axis of the fallout pattern. In addition, several stations were located upwind at 280 degrees and crosswind at 220 degrees to give a more complete picture of the fallout pattern. Station locations were chosen close to those of Projects 2.5.1 and 2.5.2 to permit exchange of information about missing measurements should one project be successful while the other failed.

For events wherein the decay rates of the neutron-induced activity in the vicinity of ground zero were of interest, stations were located at the vertices of an equilateral triangle centered on the expected location of ground zero. The distance from ground zero to the station was determined by the expected survival capability of the instrument in that overpressure region. The electronic components of the instruments were buried 2 feet below the surface. This plan of operation was chosen on site when the original plan to place the instruments in the resulting radiation field after zero time was considered too dangerous from a Rad-Safe point of view. Thus, the instruments were not designed to withstand a high overpressure, nor were they made of materials that were invulnerable to activation by neutron bombardment.

2.2 INSTRUMENTATION

The Appendix gives a detailed description of the instruments. Two main types were used: a scintillation detector for measuring high gamma-radiation rates, and an ion-chamber detector for measuring both high- and low-gamma-radiation rates. The scintillation- and ionization-type instruments were similar in construction and operation except for the use of different sensitive elements (see Appendix). The instruments required no external power nor timing signals. A recording-time capacity 24 hours greater than necessary made it possible to eliminate elaborate timing systems and requirements by starting the instruments on D – 1 day. The data were recorded on an Esterline-Angus recording milliammeter modified to use Teledeltos, a dry-writing, electrosensitive chart paper. A chart speed of 6 in/hr should have provided a resolution of 1 minute in 24 hours. Results will show this was not the case under field conditions.

An experimental cadmium-sulfide (CdS) detector was used with the regular instruments to check its behavior under field conditions for possible use on future tests, should its operation be satisfactory.

An ionization-chamber detector and a lab-built recorder mounted in the center of a large beach ball were thrown into the Shot Ess crater on D + 5 days.

2.2.1 Scintillation Detector. The detecting element of this system, a stilbene crystal in a bakelite holder, was mounted with the photomultiplier tube in a blast-resistant housing approximately 3 feet above ground level. The photomultiplier tube was used in a 100 percent feedback circuit that held the photomultiplier tube current substantially constant (regardless of the inci-

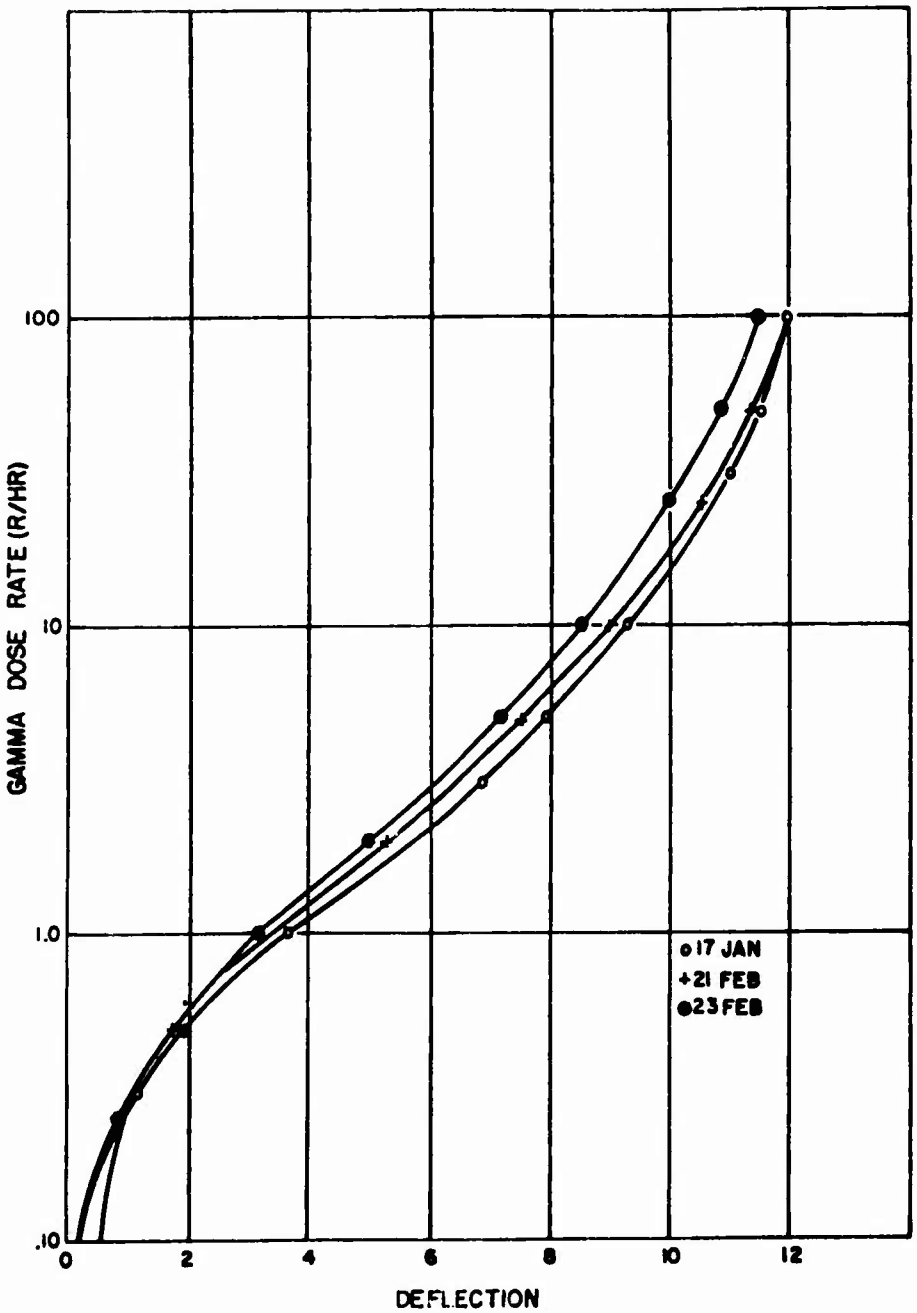

Figure 2.1 Calibration drift of Ionization Chamber P.

dent light) by varying the dynode voltage. The gain of the photomultiplier tube was approximately a function of the antilog of the dynode voltage, providing a useful dynamic range of about 10^9, if desired. The instruments were designed to cover the ranges from about 10 r/hr to 10^4 r/hr, or from 10^2 r/hr to 10^6 r/hr.

2.2.2 Ion-Chamber Detector. The detecting element of this system was an ion chamber with its associated electrometer circuit mounted in a blast-resistant housing about 3 feet above the ground. Utilization of the nonlinear characteristic of an ion chamber in the unsaturated region provided a voltage output approximately proportional to the log of the gamma radiation rate and a dynamic range of about 10^4. For these tests, two types of instruments were constructed: a low-range unit covering from 10^{-1} r/hr to 10^2 r/hr, and a high-range unit covering from 10 r/hr to 10^4 r/hr.

2.2.3 CdS Detector. A photoconducting CdS crystal (40-mm^2 area, 0.1-mm thick) was placed in series with a current-limiting resistor, a 0-to-1-milliammeter movement of an Esterline-Angus recorder, and a 300-volt battery. The CdS crystal was shielded from light and from electrons up to an energy of 1 Mev, so that essentially only gamma rays would be detected by the crystal.

2.3 CALIBRATION OF INSTRUMENTS

The low-range detector systems were directly calibrated with a 72.5-curie Co^{60} source. Calibrations were made before an event to check for proper operation of instruments before installation. Immediately after recovery, instruments were calibrated again. This calibration was used to determine the rate-versus-time results. Prior to the operation, the high-range instruments were calibrated at Evans Area, USASRDL, on a 2-Mev Van de Graaff generator. The highest rate possible with this accelerator was 10^6 r/hr. The field calibration of the high-range instruments was, of necessity, only on the lower portion of the intensity-versus-deflection curve. An investigation of the calibration drift was conducted, and the results for Detector P are shown in Figure 2.1. The laboratory calibration using fresh batteries matched the field calibration, which also used fresh batteries. Continuous operation of the instruments for two days shifted the calibration at high intensities, while the zero readings remained the same. The variation among instruments was small. If the instruments had behaved in this manner while exposed to radiation from a nuclear detonation, an estimated calibration curve at zero time could have been used. However, exposure to Shot Wasp showed that the zero also drifted down scale. To facilitate the reading of this zero drift, some instruments had their mechanical zero set at one division (12 divisions full scale) for calibration and shot participation. Figure 2.2 shows a preshot and postshot calibration for Detector P on Shot Ess. It might be argued that since zero time was halfway between preshot and postshot calibration, a calibration curve using half the drift would be best. Because this procedure would be at best a guess and because the zero drift could not be duplicated in the laboratory, the postshot calibration was used to convert deflection to dose rate. The high-range calibrations were, when necessary, extrapolated from field calibrations at low rates.

It should be noted that the inherent error of a meter (a given percentage of full-scale deflection) is multiplied when a log circuit is employed. To a close approximation, when using an n-decade log scale on a meter with an a-percent accuracy, the error is 2.3 na percent. The recorders used have an accuracy of about 2 percent, and when used with a 3-decade log circuit, they lead to a meter error alone of approximately 14 percent at full scale.

2.4 LOCATION OF INSTRUMENTS

Table 2.1, Instrumentation, lists the location of every station for every event in which Proj-

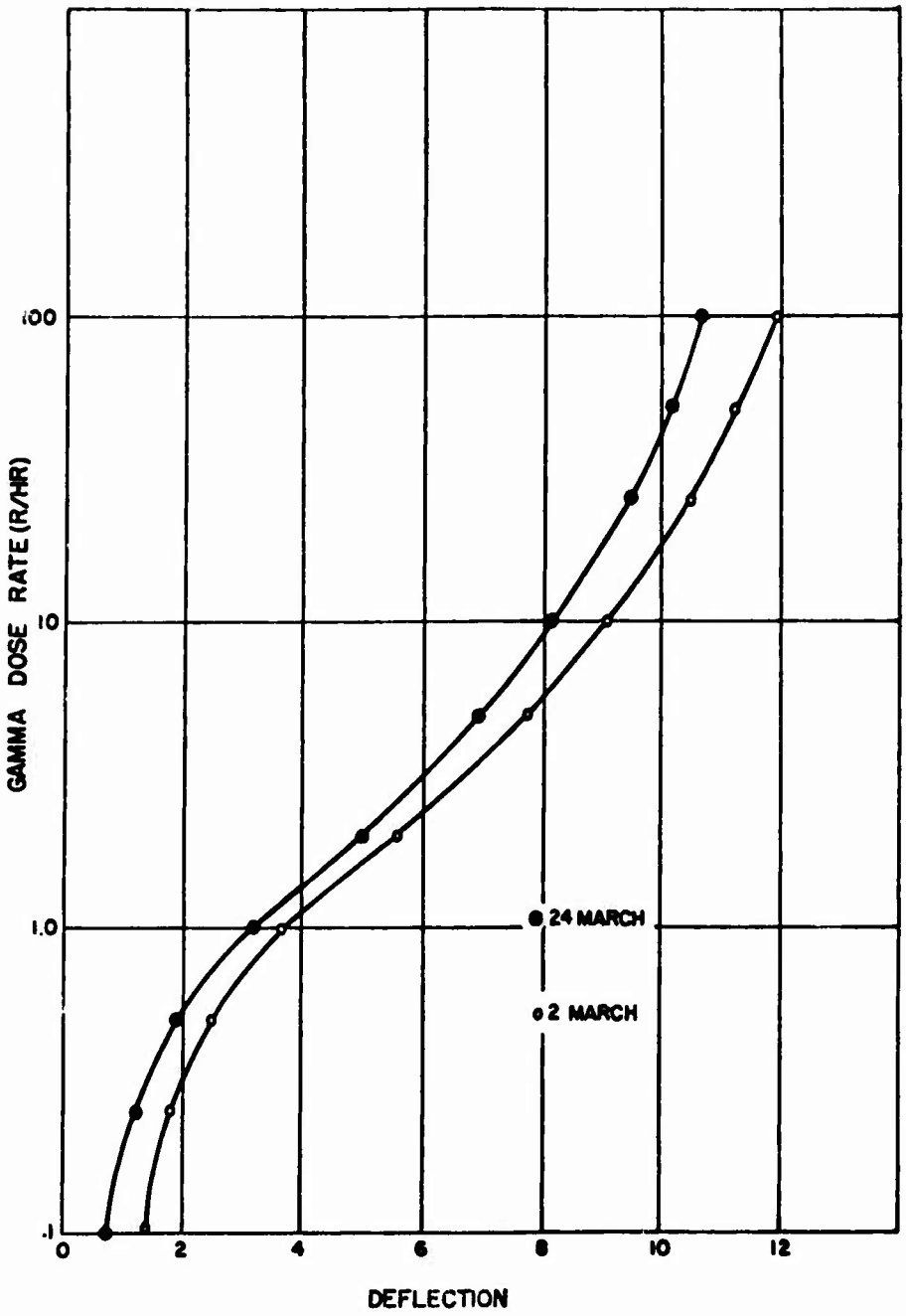

Figure 2.2 Calibration drift of Ionization Chamber P, before and after Shot Ess.

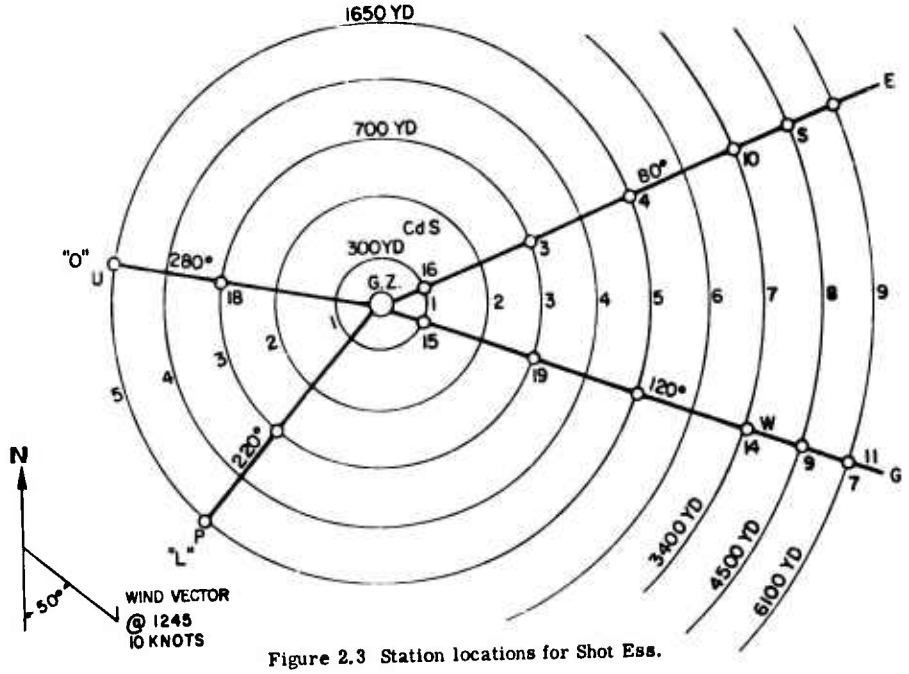

Figure 2.3 Station locations for Shot Ess.

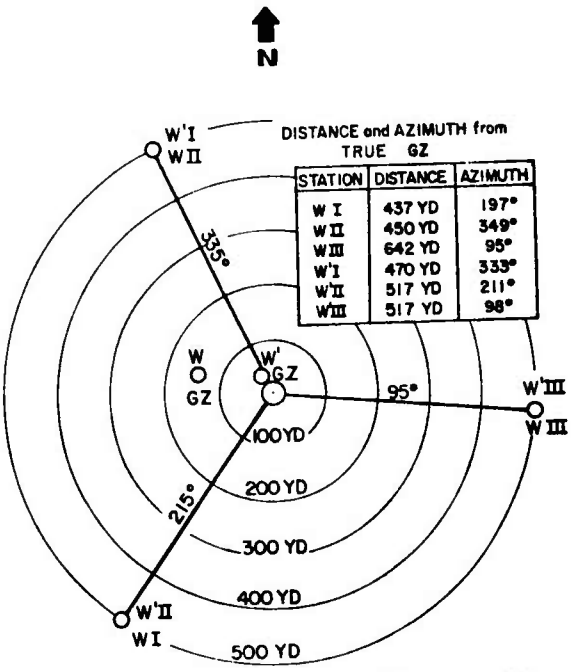

Figure 2.4 Station locations for Shots Wasp and Wasp'.

TABLE 2.1 INSTRUMENTATION

Shot Number	Station	Distance to Ground Zero	Azimuth from Ground Zero (True North)	Instrument	Figure Number	Remarks
		yd	degrees			
1	W-I	437	197	Ion chamber T	3.20	Operation satisfactory
1	W-II	450	349	Ion chamber X	—	Recorder failed
1	W-III	642	95	Ion chamber S	3.21	Operation satisfactory
2	M-II	300	25	Scintillation Detector No. 2	—	Damaged by shock
2	M-III	300	25	Ion chamber P	3.25	Operation satisfactory
2	M-IV	300	135	Ion chamber G	—	Damaged by blast
3	T-I	400	30	Ion chamber R	—	Damaged by blast
3	T-II	400	75	Scintillation Detector No. 7	—	Damaged by blast
3	T-III	300	110	Scintillation Detector No. 6	—	Damaged by blast
7	E-1(2.4a-1)	300	80	CdS	3.13	Operated
7	E-1(2.4a-1)	300	80	Scintillation Detector No. 16	3.12	Operation satisfactory
7	G-1(2.4a-2)	300	120	Scintillation Detector No. 15	3.1	Operation satisfactory
7	G-1(2.4a-2)	300	120	Scintillation Detector No. 8	—	Recorder failed
7	E-3(2.4a-3)	700	80	Scintillation Detector No. 17	—	Tube failed
7	E-3(2.4a-3)	700	80	Scintillation Detector No. 3	3.2	Operation satisfactory
7	G-3(2.4a-4)	700	120	Scintillation Detector No. 19	3.14	Operation satisfactory
7	L-3(2.4a-5)	700	220	Scintillation Detector No. 2	—	Detector failed
7	O-3(2.4a-6)	700	280	Scintillation Detector No. 13	—	Recorder failed
7	O-3(2.4a-6)	700	280	Scintillation Detector No. 18	3.3	Operation satisfactory
7	E-5(2.4a-7)	1,650	80	Scintillation Detector No. 4	3.4	Operation satisfactory
7	E-5(2.4a-7)	1,650	80	Scintillation Detector No. 12	—	Detector failed
7	O-5(2.4a-9)	1,650	220	Ion chamber P	3.5	Operation satisfactory
7	L-5(2.4a-10)	1,650	280	Ion chamber U	3.6	Operation satisfactory
7	E-7(2.4a-11)	3,400	80	Scintillation Detector No. 10	3.7	Operation satisfactory
7	G-7(2.4a-12)	3,400	120	Scintillation Detector No. 14	3.8	Operation satisfactory
7	G-7(2.4a-12)	3,400	120	Ion chamber W	3.8	Operation satisfactory
7	E-8(2.4a-13)	4,500	80	Ion chamber S	3.9	Operation satisfactory
7	E-8(2.4a-13)	4,500	80	Scintillation Detector No. 6	—	Recorder failed
7	G-8(2.4a-14)	4,500	120	Scintillation Detector No. 9	3.10	Operation satisfactory
7	G-8(2.4a-14)	4,500	120	Scintillation Detector No. 1	—	Recorder failed
7	E-9(2.4a-15)	6,100	80	Ion chamber X	—	Recorder failed
7	E-9(2.4a-15)	6,100	80	Scintillation Detector No. 5	—	Instruments below range
7	G-9(2.4a-16)	6,100	120	Scintillation Detector No. 7	3.11	Operation satisfactory
7	G-9(2.4a-16)	6,100	120	Scintillation Detector No. 11	3.11	Operation satisfactory
9	W'-I	470	333	Scintillation Detector No. 3	3.22	Operation satisfactory
9	W'-II	517	211	Scintillation Detector No. 13	3.23	Operation satisfactory
9	W'-III	518	98	Ion chamber U	3.24	Operation satisfactory

TABLE 2.2 GENERAL SHOT INFORMATION

Shot Number	Shot Name	Yield	Time*	Area	Type	Latitude and Longitude of Ground Zero
		kt				
1	Wasp	1.2	1200	T-7-4†	762-foot Air	37° 05′ 11.6856″ 116° 01′ 18.7366″
2	Moth	2.5	0545	T-3	300-foot Tower	37° 02′ 62.2654″ 116° 01′ 15.6967″
3	Tesla	7.0	0530	T-9b	300-foot Tower	37° 07′ 31.5737″ 116° 02′ 51.0077″
7	Ess	1.2	1230	T-10a	67-foot Underground	37° 10′ 06.1263″ 116° 02′ 37.7010″
9	Wasp'	3.1	1000	T-7-4‡	740-foot Air	37° 05′ 11.6856″ 116° 01′ 18.7366″

* Pacific standard time.

† Actual ground zero 56 feet North, 426 feet West of T-7-4.

‡ Actual ground zero 94 feet North, 62 feet West of T-7-4.

ect 2.4 participated, the instrument serial number, whether it functioned, and, for those instruments that gave data, the figure number of the appropriate graph.

The locations of stations used on Shot Ess are shown in Figure 2.3. The stations that yielded data show the instruments used in the corresponding location.

Figure 2.4 gives the locations of stations used on Shots Wasp and Wasp'.

2.5 SHOT PARTICIPATION

Table 2.2 summarizes the general shot information for the events pertinent to Project 2.4.

Shot participation can be divided into three categories: (1) documentation of residual fields resulting from the underground shot (Shot Ess), (2) recording of decay rates of neutron-induced fields for Shots Wasp and Wasp', and (3) measurement of residual fields from Shots Moth and Tesla (undertaken at the request of the Program Director).

Chapter 3
RESULTS and DISCUSSION

This chapter is divided into two parts: the underground burst, Shot Ess, and the air bursts, Shots Wasp and Wasp'. The underground-burst data is presented on log-log plots to permit the illustration of a power-law ($t^{-1.2}$) type of decay. The air-burst results, on the other hand, are plotted on semilog paper to facilitate the determination of half lives, an exponential type of decay.

Since Shot Moth data is similar in nature to that of the air bursts, it is plotted on semilog paper.

3.1 UNDERGROUND BURST

One of the important pieces of information that a dose-rate-versus-time plot should give is the time of arrival of activity. The Esterline-Angus clock mechanism should have been able to give the arrival time within one minute. However, in checking this accuracy, it was found that the arrival time could not be determined accurately from the tape. Detectors 7 and 11, located at the same station, were started at the same time, but according to the record the peak intensity detected by No. 7 was 11 minutes after that detected by No. 11 (Table 3.1). The shape of the curves and the peak intensity were similar; thus there can be no doubt that the arrival time was the uncertain quantity. For this reason the data for Detectors 7 and 11 (Figure 3.11) was given with the peaks arriving at the same time, even though the record indicated that this did not occur. Detectors W and 14 were also located at the same station. Here the arrival time differed by only 0.5 minute, but another malfunction in the Esterline-Angus clock transport was indicated. Figure 3.8 shows that the decay portion of the Detector W curve occurred about 735 minutes after that of the Detector 14 curve. A comparison of the arrival of peak rate could not be made since Detector W went off scale for a time. A possible explanation for this delay was that the tape jumped 735 minutes after being hung up for this length of time. The CdS detector and No. 16, located at the same station, showed a difference of arrival time of 22.5 minutes. No. 16 showed an arrival time of minus 3.5 minutes (before shot time), a further indication of the inaccuracy of the recorder tape transport. Since this station was only 300 yards from ground zero, the arrival of activity should have been close to zero time.

Table 3.2 gives a comparison between Project 2.5.1 (Reference 13) and Project 2.4 arrival times for the same location. The two stations at 3,400 yards from ground zero show good agreement between Project 2.5.1 arrival time and Project 2.4 peak-activity arrival time. Comparison of arrival times at other stations, however, points out the lack of accuracy of the Esterline-Angus clock movement under field conditions.

The data from Shot Ess are shown in Figures 3.1 through 3.18. The intensity-versus-time curves plotted on log-log paper have certain similarities. After reaching a maximum, the curves decayed rapidly for a few minutes and then settled down to approximately a power-law decay with slopes from -1.2 to -1.4. If the decay were truly a power-law type, the equation for the dose rate D at time t would take this form:

$$D = At^m \qquad (3.1)$$

or $$\log D = m \log t + \log A$$

(Text continued on pag. 26)

TABLE 3.1 VARIATIONS IN RECORDED ARRIVAL TIMES, SHOT ESS

Detector Number	Clocked Start to Zero		From Tape: Arrival Time of First Deflection from Start of Recorder		From Tape: Arrival Time of Peak Deflection from Start of Recorder		Maximum Deflection	Peak Rate
	hour	minute	hour	minute	hour	minute		r/hr
7	17	0	17	12.5	17	15	5.1	230
11	17	0	17	2.5	17	4	5.9	235
W	17	50	17	50	—	—	—	Off scale
14	17	50	17	50.5	17	54	11.65	1.85×10^3
Cd5	21	30	21	49	—	—	12.75	Off scale
16	21	30	21	26.5	21	26.5	11.55	1.42×10^5

TABLE 3.2 COMPARISON OF ARRIVAL TIMES, PROJECTS 2.4 AND 2.5.1, SHOT ESS

Project 2.5.1				Project 2.4		
Azimuth	Distance	Station	Time of Arrival	Closest Station	Arrival of Minimum Detectable Activity	Arrival of Peak Activity
degree	yd		minute		minute	minute
100	3,400	F-7	5	No. 10	2.5	6
120	300	G-1	0.5	No. 15	<2.5	—
120	700	G-3	2.4	No. 19	0.5	0.8
120	3,400	G-7	5	W	0	—
120	3,400	G-7	5	No. 14	0.5	4.5
140	4,500	H-8	5	No. 9	0.5	1.7

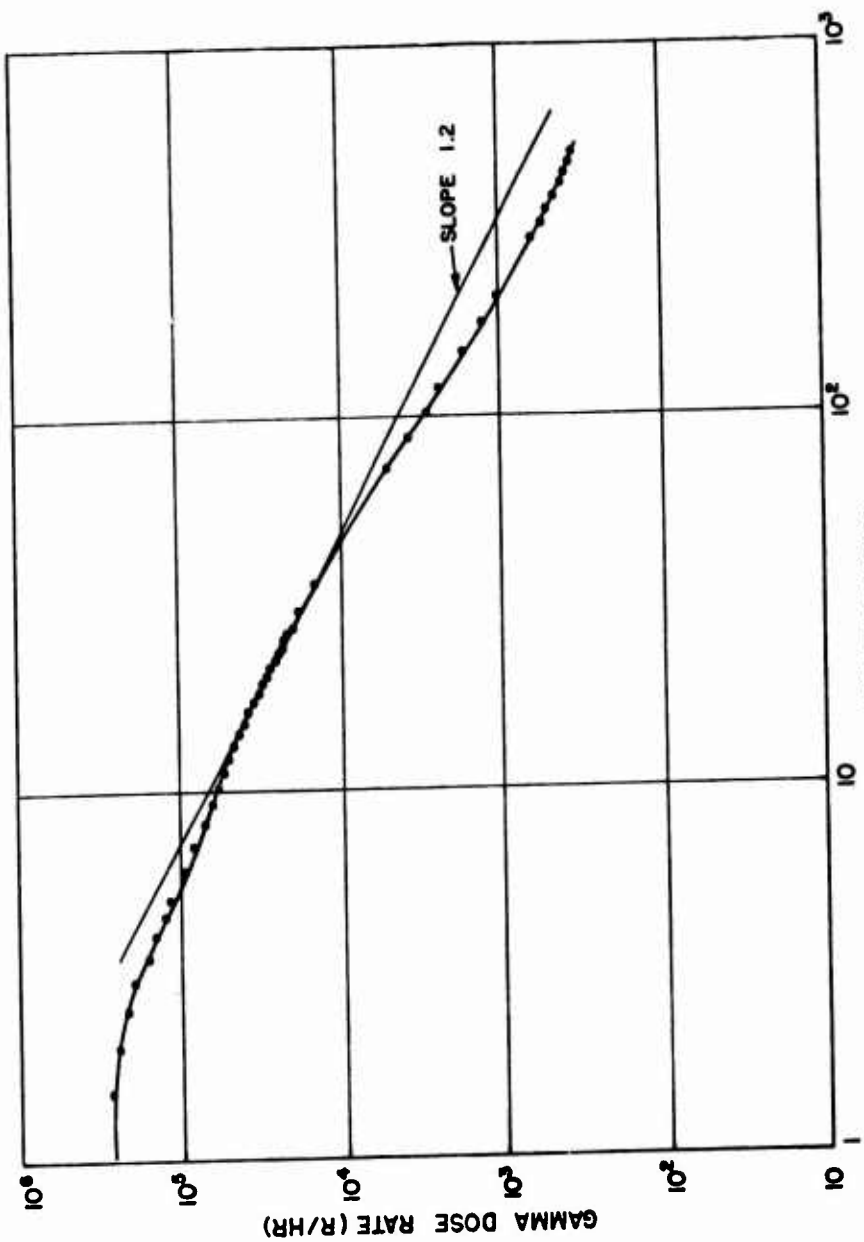

Figure 3.1 Intensity-versus-time curve, Shot Ess, Scintillation Detector 15, 300 yards, 120 degrees.

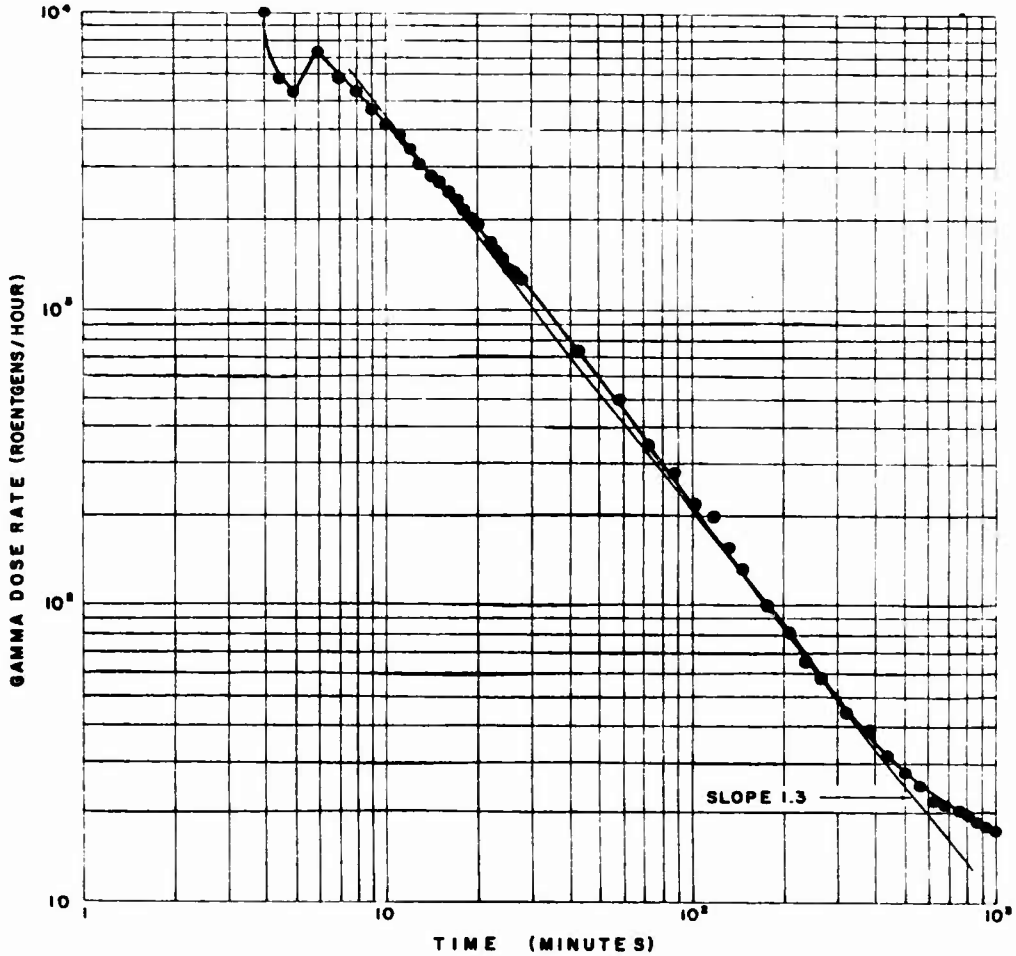

Figure 3.2 Intensity-versus-time curve, Shot Ess, Scintillation Detector 3, 700 yards, 80 degrees.

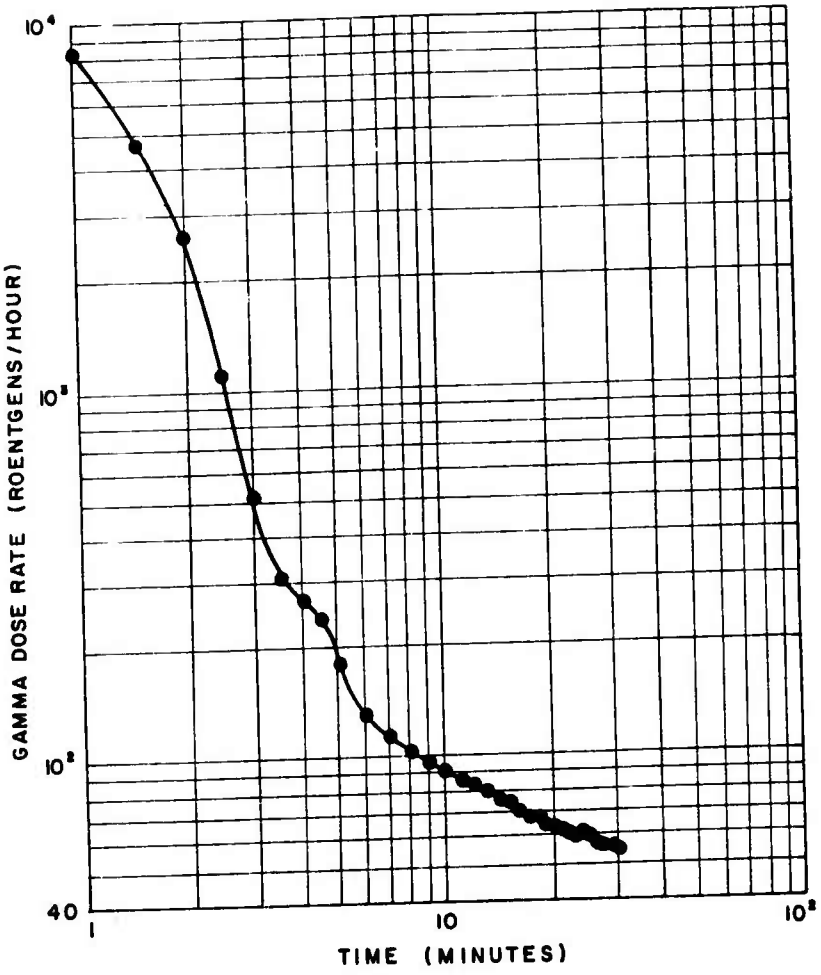

Figure 3.3 Intensity-versus-time curve, Shot Ess, Scintillation Detector 18, 700 yards, 280 degrees.

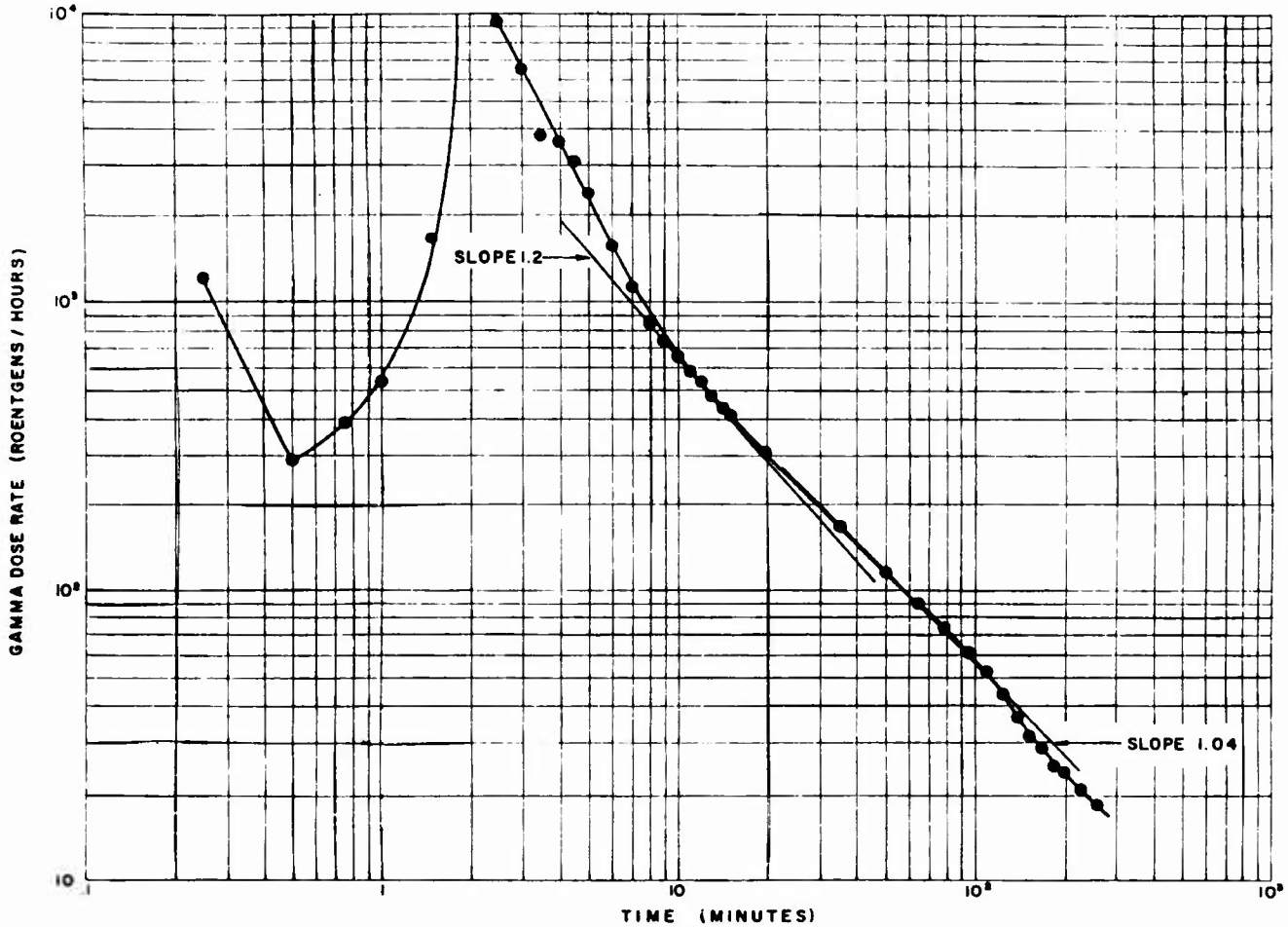

Figure 3.4 Intensity-versus-time curve, Shot Ess, Scintillation Detector 4, 1,650 yards, 80 degrees.

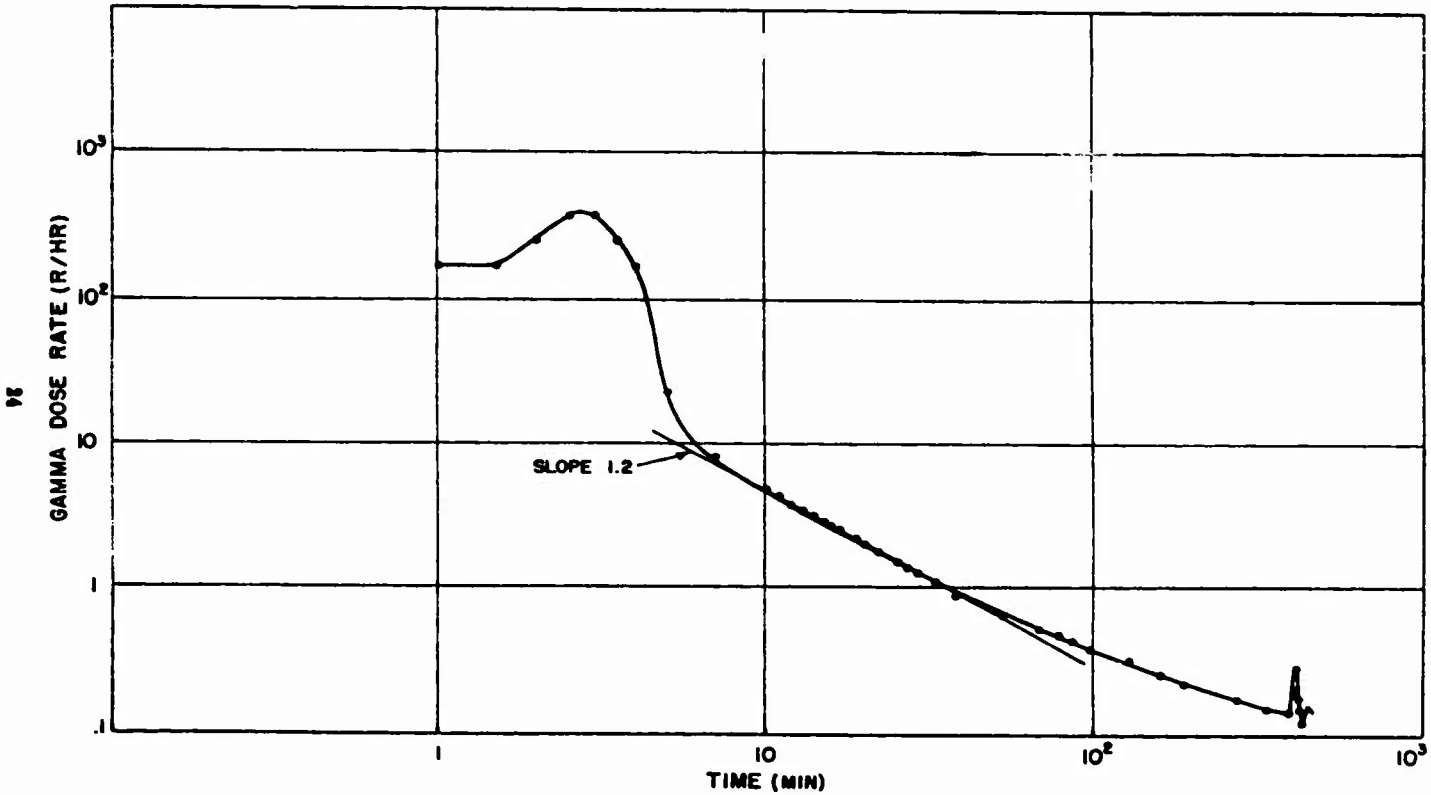

Figure 3.5 Intensity-versus-time curve, Shot Ess, Ionization Chamber P, 1,650 yards, 220 degrees.

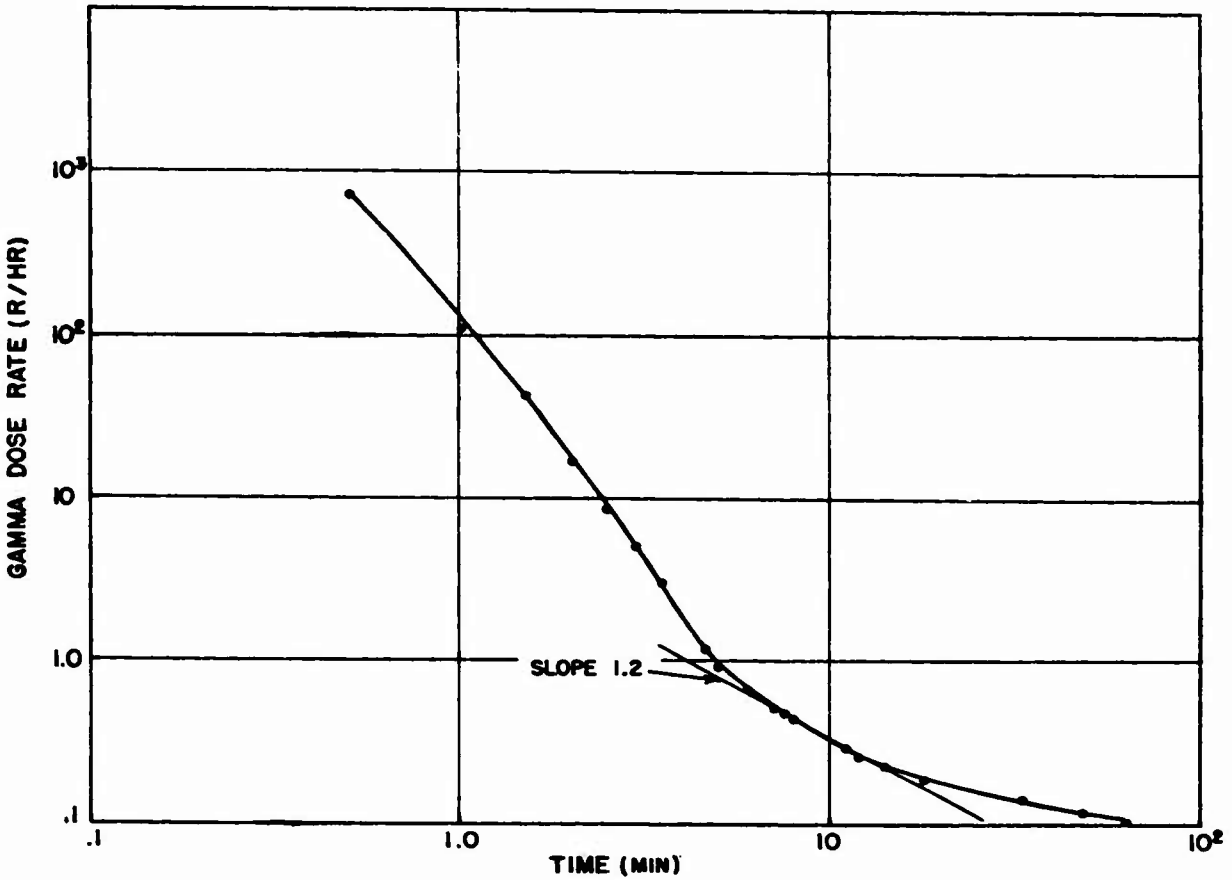

Figure 3.6 Intensity-versus-time curve, Shot Ess, Ionization Chamber U, 1,650 yards, 280 degrees.

which would be a straight line on log-log paper with a slope m and an intercept log A.

A straight line was therefore fitted to the part of the curve that showed power-law behavior. Taking two points on this straight line, (D_1, t_1) and (D_2, t_2), the slope was determined by using the following expression:

$$m = \frac{\log (D_1/D_2)}{\log (t_1/t_2)} \tag{3.2}$$

For comparison purposes, the straight line that was used to determine the slope is drawn on the same plot as the data.

The rapid decay observed in the data curves immediately after the maximum dose rate was reached, was attributed to the passage of the air-borne debris past the detector station. The

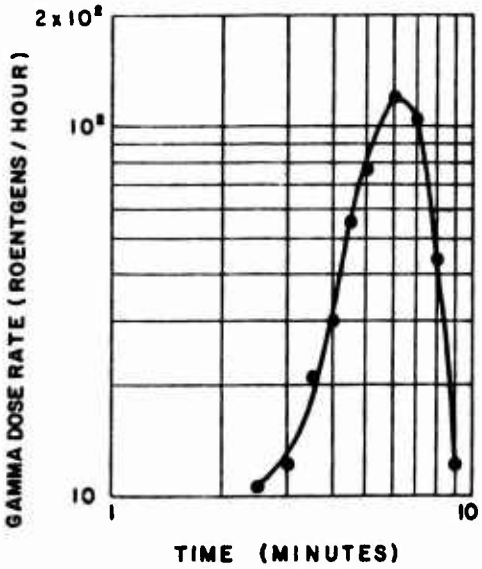

Figure 3.7 Intensity-versus-time curve, Shot Ess, Scintillation Detector 10, 3,400 yards, 80 degrees.

initial rise and very early decay of the dose rate was that which would be expected from the arrival and passage of a contaminated air volume. Since a portion of the air-borne debris was deposited on the ground during this passage, the dose rate decay subsequent to the departure of the contaminated volume represented the actual decay of the deposited fission product contaminant. The apparent early rapid decay was consistent with the movement of the radioactive cloud under influence of the 10-knot wind which existed at shot time.

Instruments located along the 80- and 120-degree lines from 300 to 1,650 yards showed a slight bulge in the decay curve from 10 minutes to about 150 minutes. Figures 3.1, 3.2, 3.4, 3.12, and 3.14 show this behavior. Since five different instruments show this effect and furthermore are located in the same area, the effect must be real. No explanation has been found for this behavior.

As a rough check of the accuracy of the dose rate, a graphic integration of dose rate over the total recording time was made to get the total dose. Table 3.3 compares Project 2.4 integrated

(Text continued on page 35)

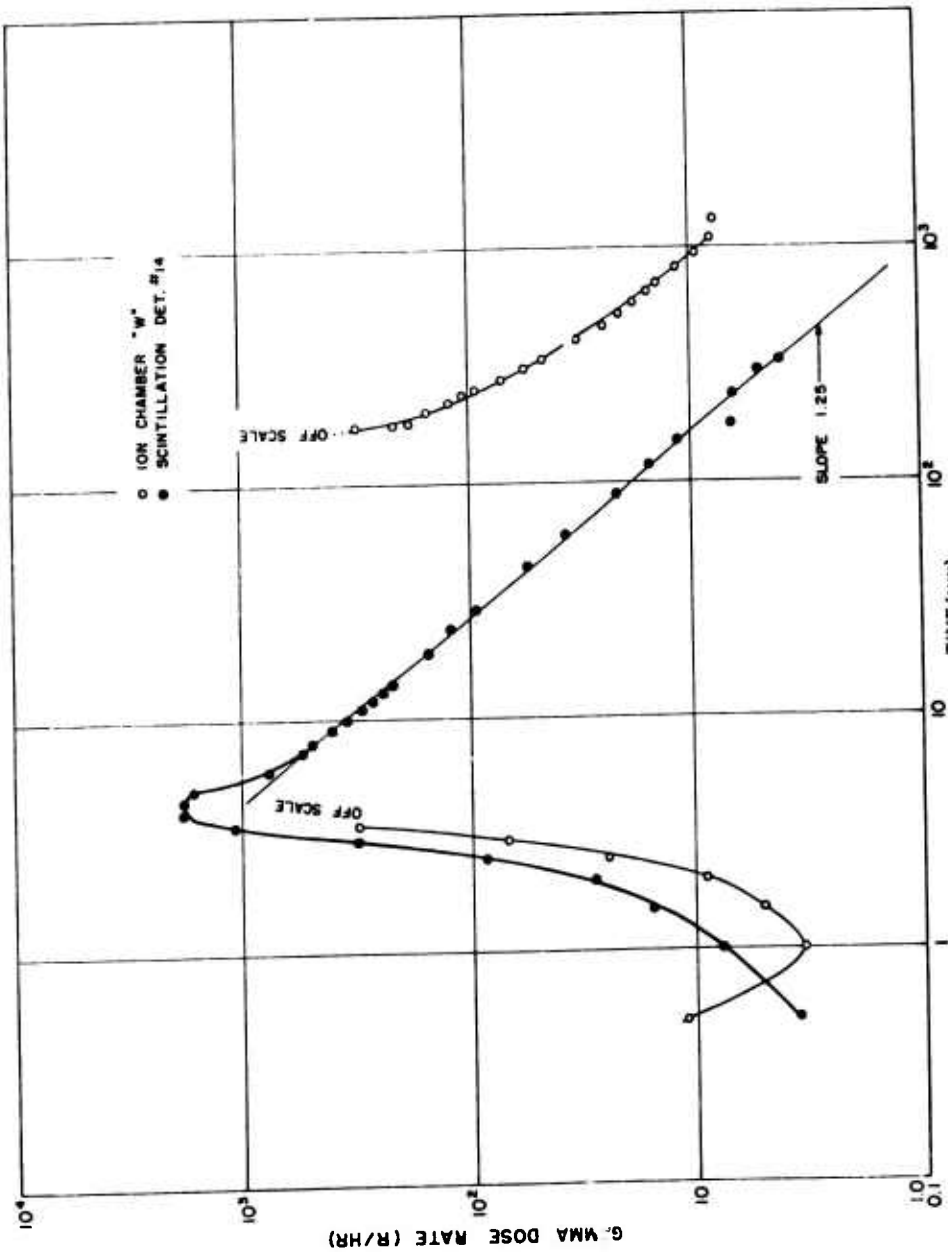

Figure 3.8 Intensity-versus-time curve, Shot Ess, Scintillation Detector 14, Ionization Chamber W, 3,400 yards, 120 degrees.

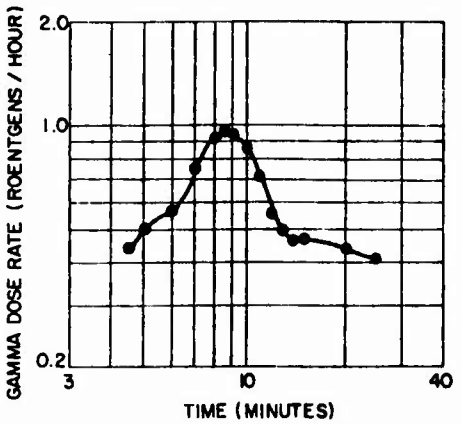

Figure 3.9 Intensity-versus-time curve, Shot Ess, Ionization Chamber S, 4,500 yards, 80 degrees.

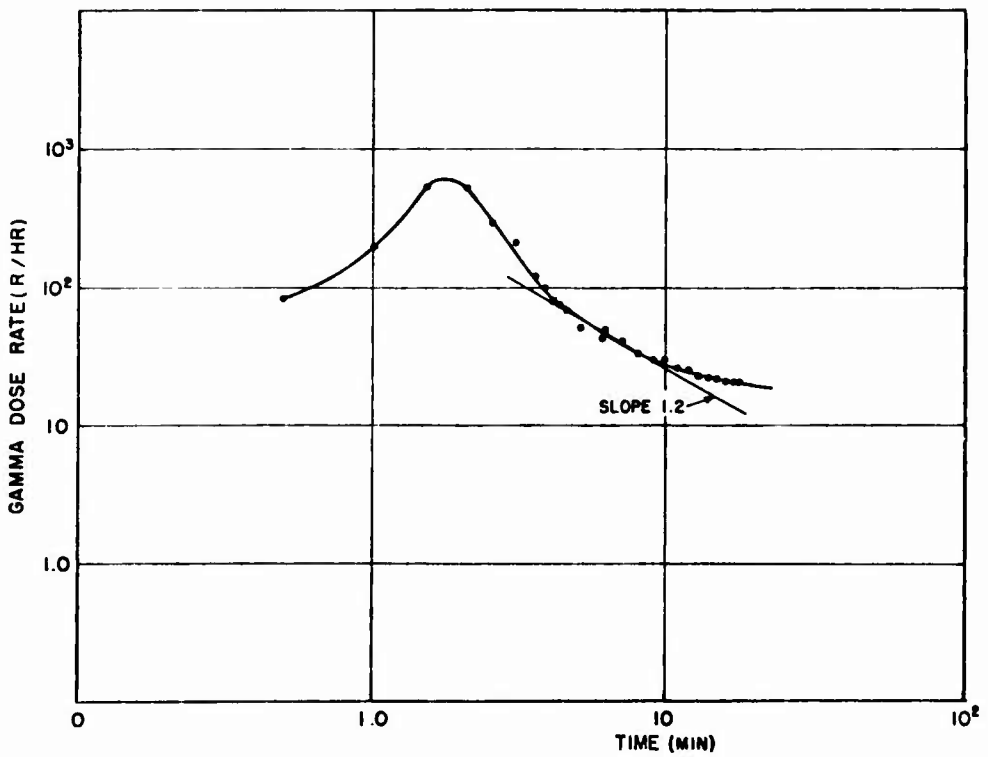

Figure 3.10 Intensity-versus-time curve, Shot Ess, Scintillation Detector 9, 4,500 yards, 120 degrees.

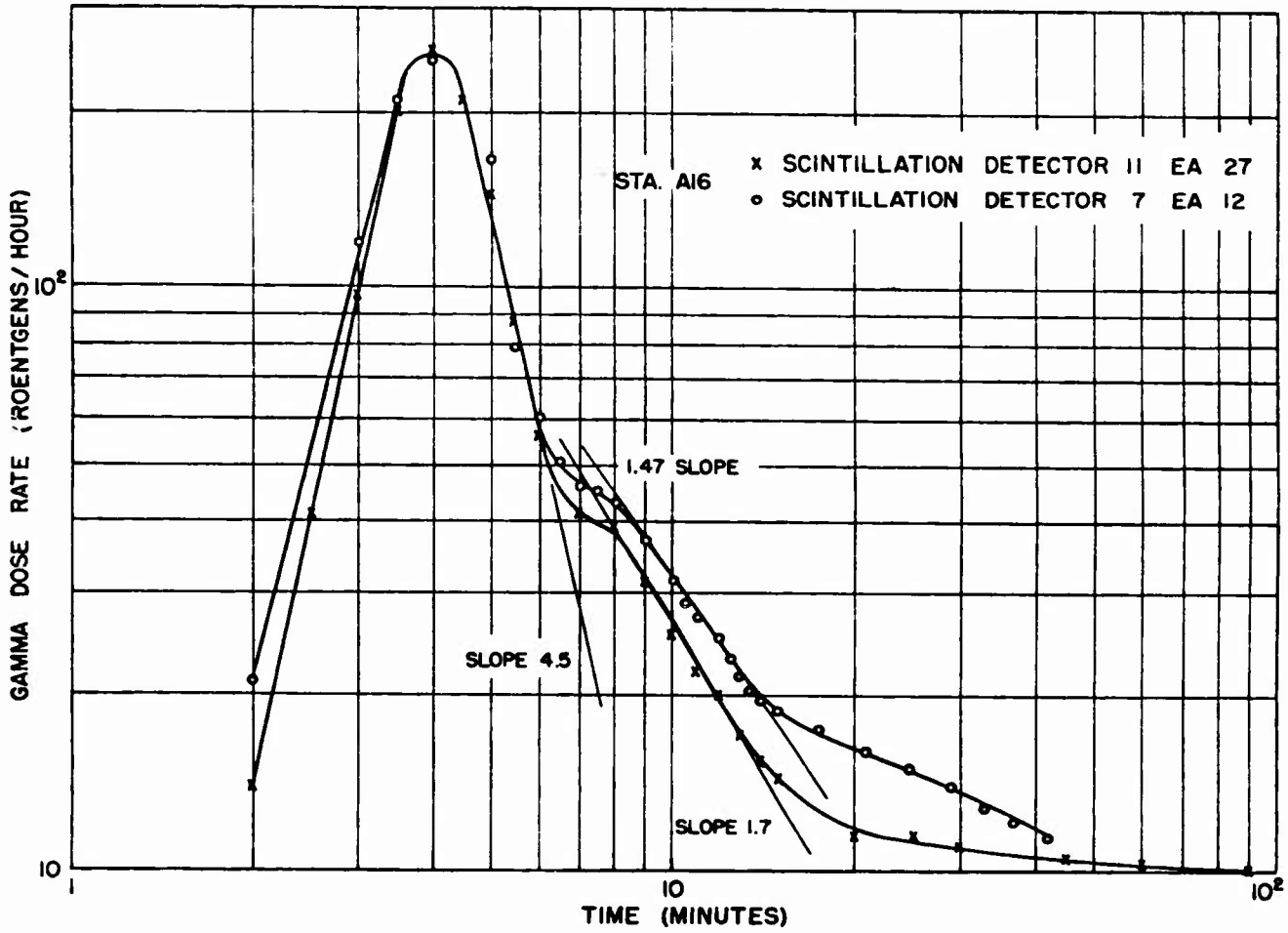

Figure 3.11 Intensity-versus-time curve, Shot Ess, Scintillation Detectors 7 and 11, 6,100 yards, 120 degrees.

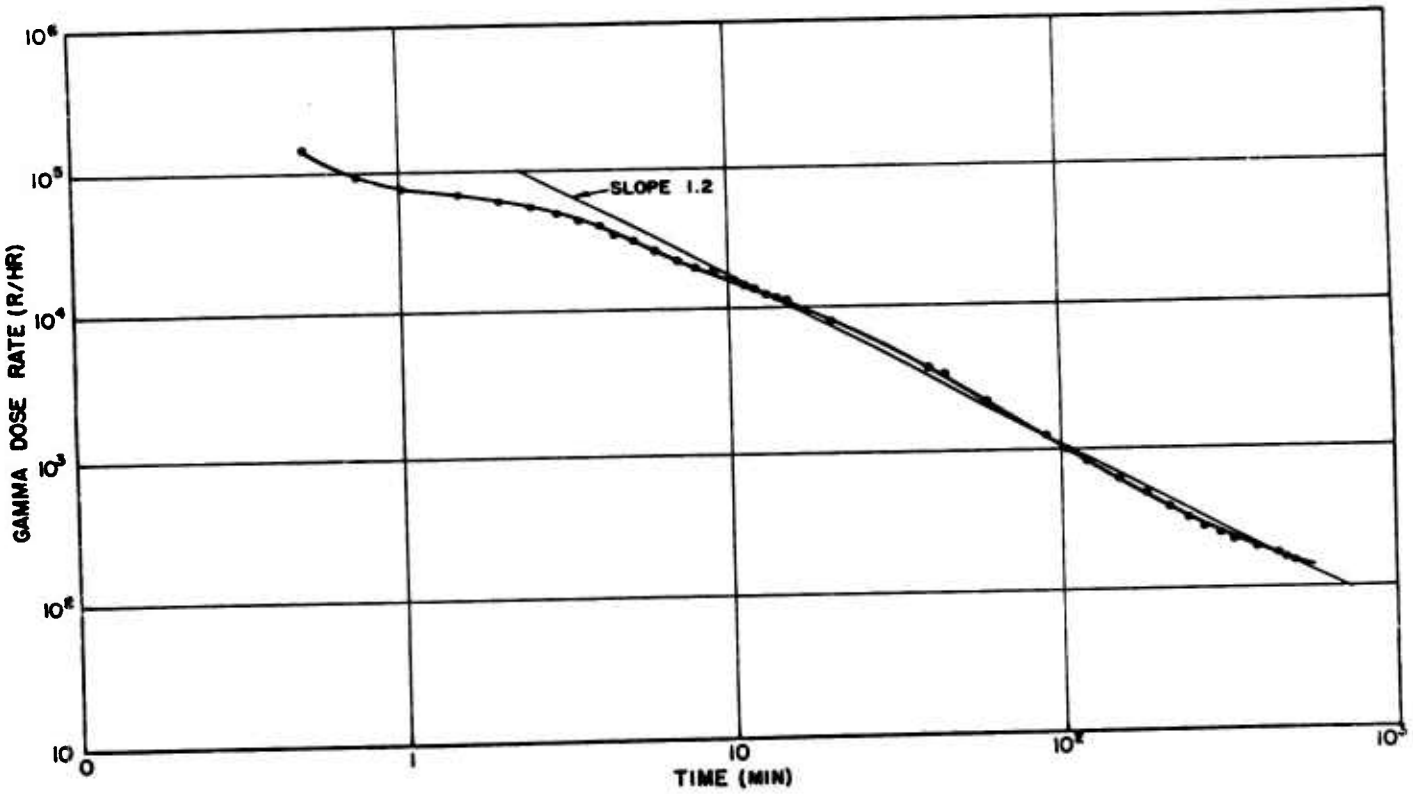

Figure 3.12 Intensity-versus-time curve, Shot Esa, Scintillation Detector 16, 300 yards, 80 degrees.

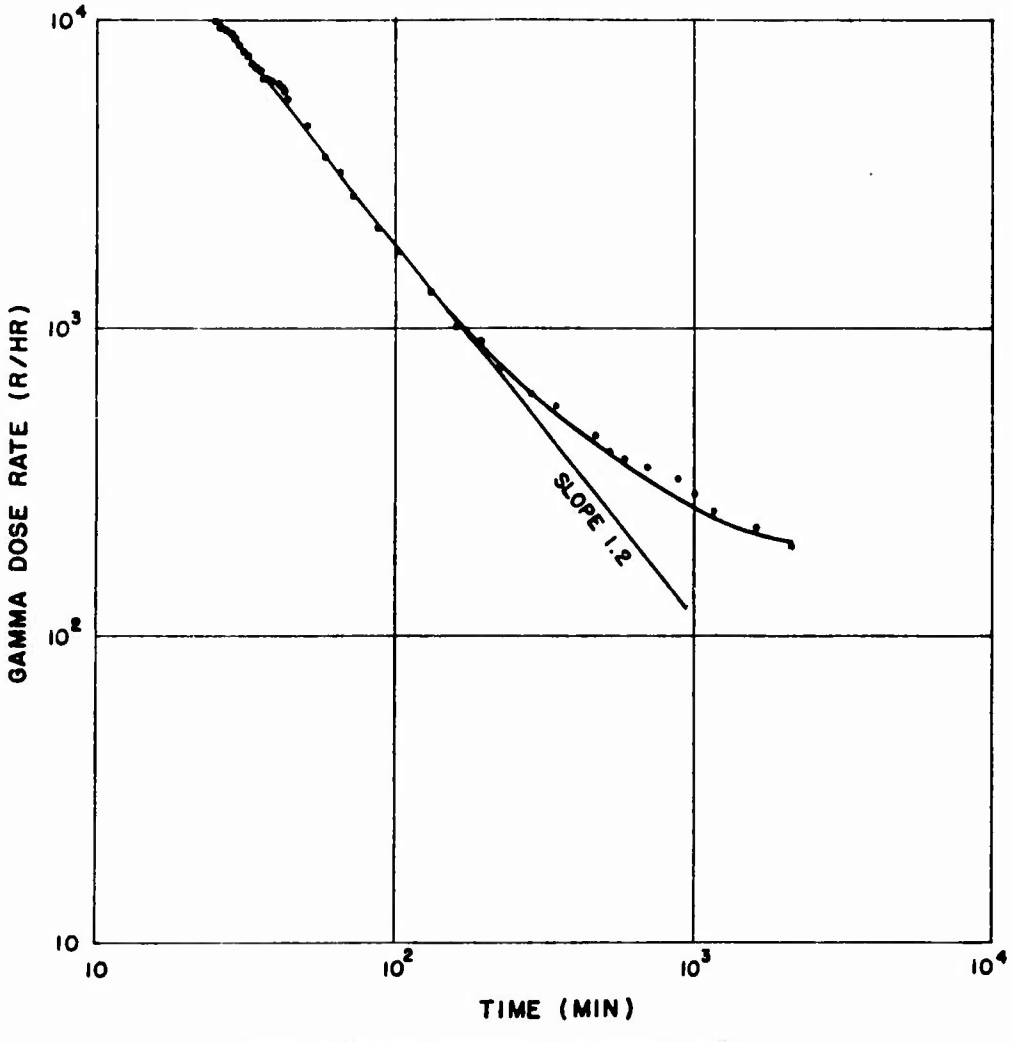

Figure 3.13 Intensity-versus-time curve, Shot Ess, Scintillation Detector CdS, 300 yards, 80 degrees.

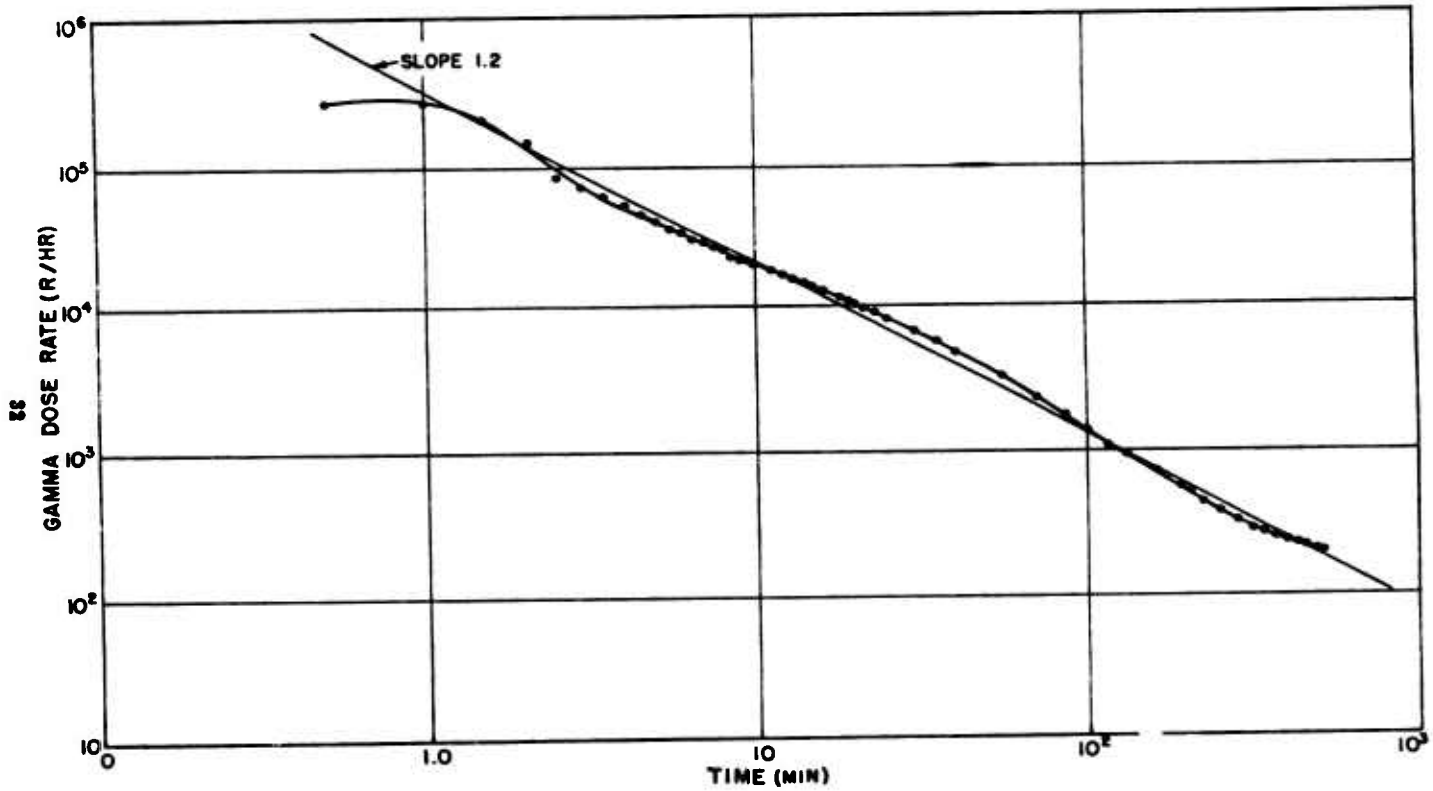

Figure 3.14 Intensity-versus-time curve, Shot Ess, Scintillation Detector 19, 700 yards, 120 degrees.

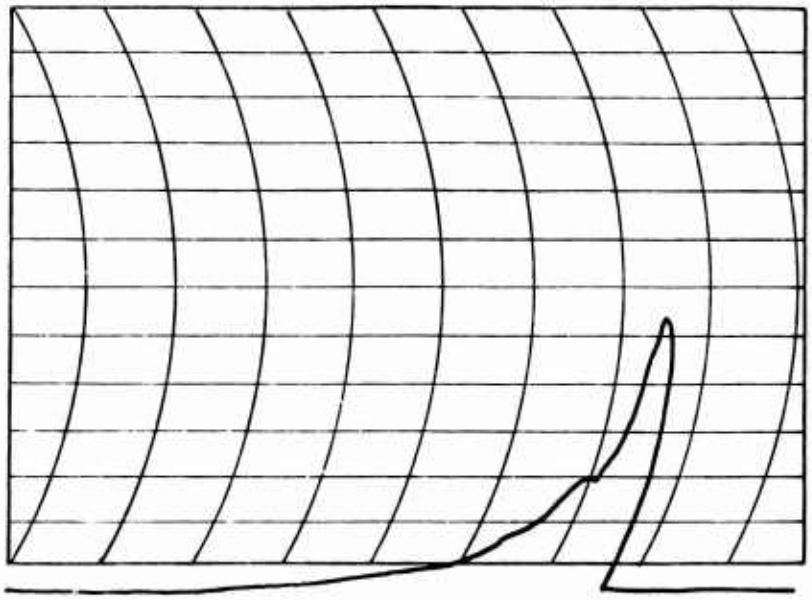

Figure 3.15 Instrument recording, Shot Ess, Scintillation Detector 11, 6,100 yards, 120 degrees.

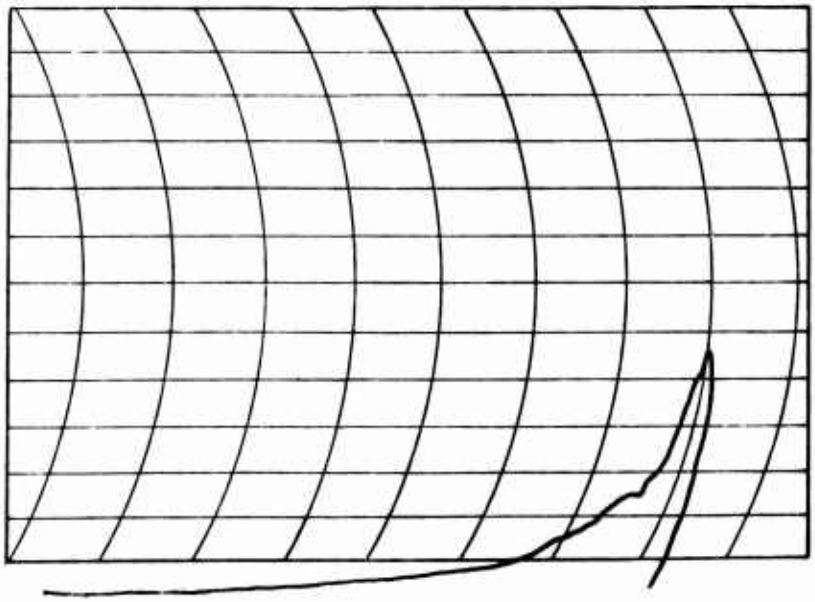

Figure 3.16 Instrument recording, Shot Ess, Scintillation Detector 7, 6,100 yards, 120 degrees.

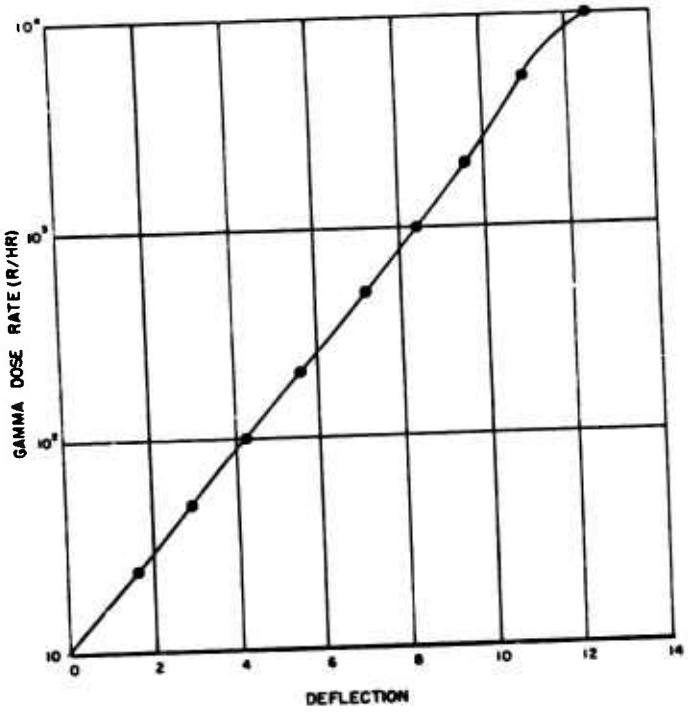

Figure 3.17 Postshot calibration curve, Shot Ess, Scintillation Detector 11, 6,100 yards, 120 degrees.

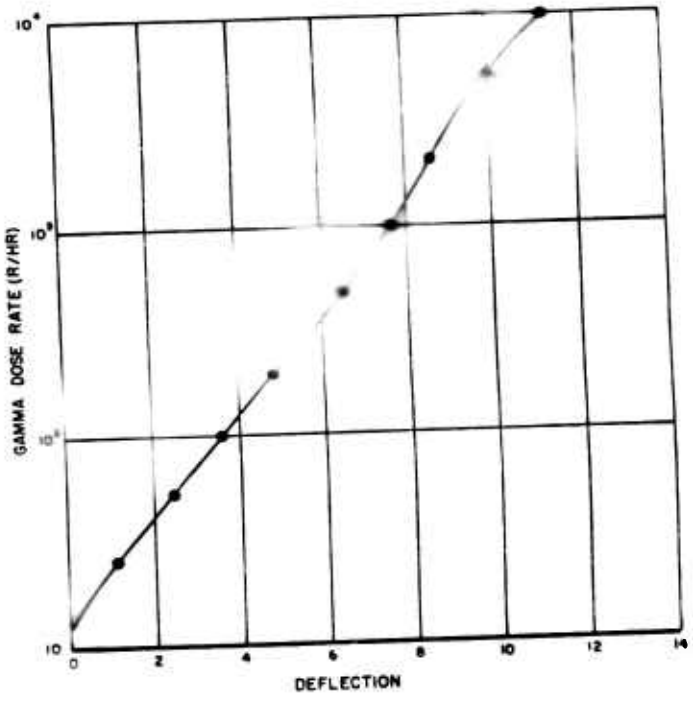

Figure 3.18 Postshot calibration curve, Shot Ess, Scintillation Detector 7, 6,100 yards, 120 degrees.

doses with those of Project 2.1 (Reference 14). (Project 2.1 measured total dose with NBS film packets.) Also shown is the beginning and end of the integration time for the Project 2.4 curves and the exposure time of the NBS film packets. The Project 2.1 total exposure is not known to better than ± 5 hours.

Detector 9 (Figure 3.10) could not be made to operate after recovery, although it functioned satisfactorily during the shot. Since a postshot calibration was therefore not available, the preshot calibration was used to convert recorded deflection to dose rates.

A sample of the data for Detectors 7 and 11, as recorded on the Esterline-Angus, is shown in Figures 3.15 and 3.16. The calibration curves (for these two instruments) that were used to

TABLE 3.3 COMPARISON OF TOTAL DOSES, PROJECTS 2.4 AND 2.1, SHOT ESS

Station	Distance	Detector Number	Project 2.4 Total Time From	Project 2.4 Total Time To	Project 2.4 Total Dose	Project 2.1 Total Time (± 5 hours)	Project 2.1 Total Dose
	yd		minute		r	hour	r
E-1	300	CdS	24	2,000	1.32×10^4	120	2.5×10^4
E-1	300	16	0.5	570	1.5×10^4	120	0.9×10^4
G-1	300	15	1.0	500	5.6×10^4	120	2.5×10^4
E-3	700	3	4.0	1,000	2.73×10^3	72	3.3×10^3
G-3	700	19	15	520	4.72×10^4	120	0.95×10^4
O-3	700	18	1.0	30.0	1.59×10^2	24	2.5×10^2
E-5	1,650	4	0.25	260	1.37×10^3	—	—
L-5	1,650	P	1.0	450	18.5	24	5.9
O-5	1,650	U	0.5	64.0	25.4	24	2.35
E-7	3,400	10	2.5	9.0	6.64	24	5×10^2
G-7	3,400	14	0.5	450	2.09×10^3	24	2.5×10^2
E-8	4,500	S	4.5	25.0	0.264	24	5×10^2
G-8	4,500	9	0.5	19.0	30.4	24	20
G-9	6,100	7	2.0	42.0	20.6	24	14
G-9	6,100	11	2.0	90.0	26.4	24	14

convert deflection to dose rate are shown in Figures 3.17 and 3.18. Tables 3.4 and 3.5 show the steps taken to obtain the data points for the dose-rate-versus-time curves in Figure 3.11. Tables 3.6 and 3.7 show the increments used to make the integration for Table 3.3.

Detector 16 (Figure 3.12) and the CdS detector (Figure 3.13) were both located at the same station. Since activity arrival times differ by about 22 minutes and both instruments are off scale initially, a comparison of dose rate at early times cannot be made. At 500 minutes after detonation, an initial difference of 20 minutes was only 4 percent of the total elapsed time, and a comparison of dose rate would be more reasonable. Detector 16 reads 156 r/hr at 500 minutes, while the CdS detector reads 390 r/hr for the same time. Of the two, Detector 16 must be considered more reliable. Figure 3.19 shows that not only does the CdS calibration change from time to time and is sensitive to polarity, but it also shows a dependence on past history. Additional research since Operation Teapot has not succeeded in producing a reliable CdS-crystal radiation detector. Crystals still show dependence on past history and batch variation. The causes of these effects are not known.

An ionization-chamber instrument mounted in a beach ball that was thrown into the Shot Ess crater on D + 5 days was never recovered. Cave-ins from the side and lip of the crater buried

TABLE 3.4 DATA READ-OUT, SHOT ESS, SCINTILLATION DETECTOR 11, 6,100 YARDS, 120 DEGREES

Time	Deflection	Dose Rate	Time	Deflection	Dose Rate
minute		r/hr	minute		r/hr
2	0.60	14.0	10	1.70	25.5
2.5	2.60	41.0	11	1.45	22.0
3	4.20	97.0	12	1.30	20.0
3.5	5.50	200.0	13	0.95	17.0
4	5.95	255.0	14	0.80	15.5
4.5	5.60	210.0	15	0.65	14.5
5	4.90	145.0	20	0.25	11.5
5.5	4.00	87.0	25	0.25	11.5
6	3.20	56.0	30	0.15	11.0
7	2.60	41.0	45	0.05	10.5
8	2.50	39.0	60	0.03	10.3
9	2.10	31.0	90	0.0	10.0

TABLE 3.5 DATA READ-OUT, SHOT ESS, SCINTILLATION DETECTOR 7, 6,100 YARDS, 120 DEGREES

Time	Deflection	Dose Rate	Time	Deflection	Dose Rate
minute		r/hr	minute		r/hr
1.5	0.0	11.5	10.5	1.35	28.5
2	0.8	21.5	11	1.2	27.0
2.5	2.0	41.0	12	1.1	25.0
3	3.9	118.0	12.5	0.9	22.8
3.5	4.9	208.0	13	0.8	21.3
4	5.25	245.0	13.5	0.7	20.0
4.5	4.9	208.0	14	0.65	19.5
5	4.5	165.0	15	0.6	18.7
5.5	3.2	79.0	17	0.5	17.5
6	2.7	60.0	21	0.4	16.0
6.5	2.4	50.0	25	0.3	15.0
7	2.2	45.5	29	0.2	14.0
7.5	2.15	45.0	33	0.1	13.0
8	2.1	43.0	37	0.05	12.25
9	1.8	37.0	42	0.0	11.5
10	1.5	31.5			

TABLE 3.6 CALCULATION OF INTEGRATED DOSE FOR TABLE 3.4, SCINTILLATION DETECTOR 11

D	Δt	DΔt	DΔt/60
r/hr	minute		r
27	0.5	13.5	0.225
79	0.5	39.50	0.658
148	0.5	74	1.233
222.5	0.2	44.50	0.742
247.5	0.3	74.25	1.238
230	0.5	115.0	1.917
170	0.5	85.0	1.41
107	0.5	53.5	0.892
66	0.7	46.2	0.770
44.5	0.8	35.60	0.593
39.5	1.0	39.5	0.658
34.5	1.0	34.5	0.575
28.5	1.0	28.5	0.475
22	2.5	55.0	0.91
15.75	2.5	39.38	0.656
12.12	5.0	60.60	1.010
11.50	5.0	57.50	0.958
11.13	5.0	55.65	0.927
10.77	15.0	161.55	2.692
10.5	45.0	472.5	7.875
		Total r	26.4

TABLE 3.7 CALCULATION OF INTEGRATED DOSE FOR TABLE 3.5, SCINTILLATION DETECTOR 7

D	Δt	DΔt	DΔt/60
r/hr	minute		r
37	0.5	18.5	0.308
81.5	0.5	40.75	0.679
160	0.5	80.0	1.333
222.5	0.2	44.50	0.742
247.5	0.3	74.25	1.238
230	0.5	115.0	1.917
170	0.5	85.0	1.410
107	0.5	53.5	0.892
68	0.7	47.6	0.793
50.5	0.8	40.4	0.673
44.5	1.0	44.5	0.742
40.0	1.0	40.0	0.667
34.25	1.0	34.25	0.571
32.25	2.5	80.62	1.344
20.88	2.5	52.20	0.870
17.37	5.0	86.85	1.448
15.37	5.0	76.85	1.281
14.25	5.0	71.25	1.188
13.25	5.0	66.25	1.104
11.87	7.0	83.09	1.385
		Total r	20.585

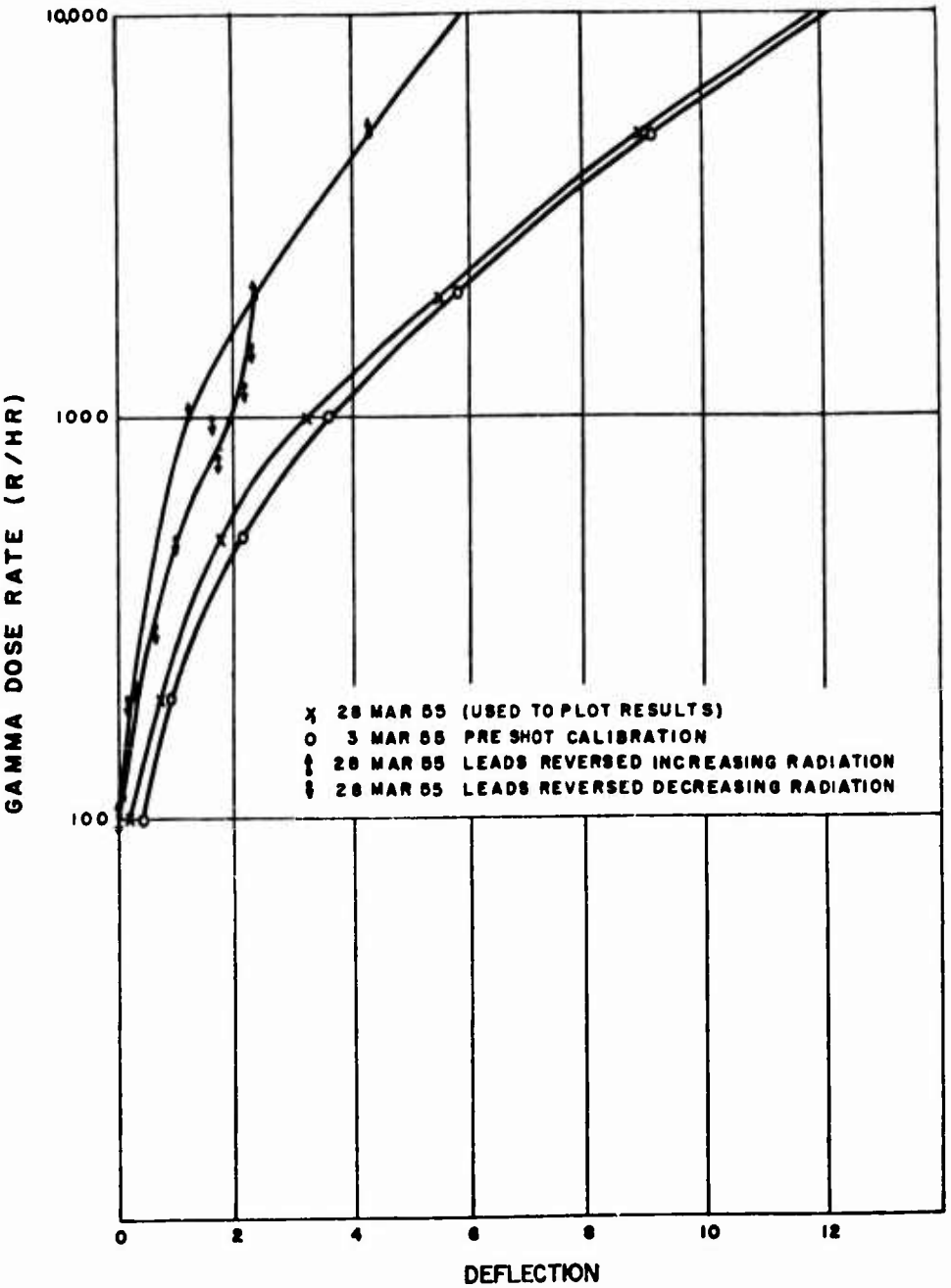

Figure 3.19 Variations in CdS calibrations.

the ball so deeply that it was not possible to pull it out with the aid of the rope that was attached to the ball. Recovery by other means was also unsuccessful.

3.2 AIR BURSTS

Data for induced activity from air-burst type shots (Shots Wasp, Wasp', and Moth) are shown in Figures 3.20 through 3.25.

Two scales were used for the abscissa on each curve to give an accurate picture of both early and late times.

The unanalyzed dose-rate-versus-time data plotted on semilog paper has the broken-line appearance of several mixed isotopes with different half lives. A graphic analysis was made in an attempt to determine the isotopes responsible for the radiation. A straight line was fitted to the part of the curve with the smallest slope and its half life determined. A new curve was then plotted by subtracting the first straight line from the original curve. A second straight line was then fitted to the linear portion of the second curve having the smallest slope. The half life of this straight line was then determined. This process was continued as far as possible with a reasonable length of curve available for analysis. The half lives, graphically determined, were compared to those of isotopes having a high relative-importance factor as determined in the manner mentioned in Chapter 1. Where these half lives were too different from the high-relative-importance-factor isotopes, other isotopes were used having half lives close to those determined from the data.

Soil analysis for Nevada soil (Reference 15) was used to compute the relative-importance factors at 10 minutes for all the isotopes listed in the analysis. The isotopes whose importance factors were not negligible are listed in Table 3.8 (References 16 and 17 were used as sources for some of the information in this table). Most of the data curves indicate the presence of Al^{28}, Mn^{56}, and either Na^{24} or K^{42}, which are isotopes having a high-importance factor. Although other isotopes are included in the graphs, the validity of their inclusion seems doubtful. It must be remembered that this technique for determining the presence of isotopes in a composition is not too accurate, even under laboratory conditions.

The analysis is further complicated because the detectors could not be shielded as thoroughly as desirable, and the detectors were also activated by the neutron flux from the device.

The instrument housings and electronics were found to be radioactive. Dr. C. S. Cook allowed the components to be analyzed, using the analytical facilities of USNRDL. He found Na^{24}, Mn^{56}, Cs^{134}, and Cu^{66} present, but because of the complexity of the problem a quantitative analysis of the components could not be made. Because of lack of quantitative information and because some of the isotopes were within the photomultiplier tubes, the contribution of the isotopes in the electronics to the total reading of the instruments could not be determined.

On the other hand, the relative contribution of the aluminum blast shield to the aluminum in the soil could be approximated since the percentage of aluminum in the soil was known and the weight and dimensions of the aluminum blast shield were also known.

The method chosen to make this comparison was to assume a dose rate from the aluminum shield at time zero. A nominal 1,000 r/hr was used (approximately that recorded in the field). The specific activity of the aluminum in the shield to give the above dose rate was next computed. The same specific activity was then used for the aluminum in an infinite plane of soil to determine the relative contribution of the soil aluminum to the detector reading. The analysis of Nevada soil (Reference 15) was used for the percentage of aluminum in the infinite-plane calculation.

The analysis of radiation from a cylindrical source is given in Reference 18; however, the nomenclature given in Reference 19 is used here. For the center of a hollow cylinder (a hollow

(Text continued on page 47)

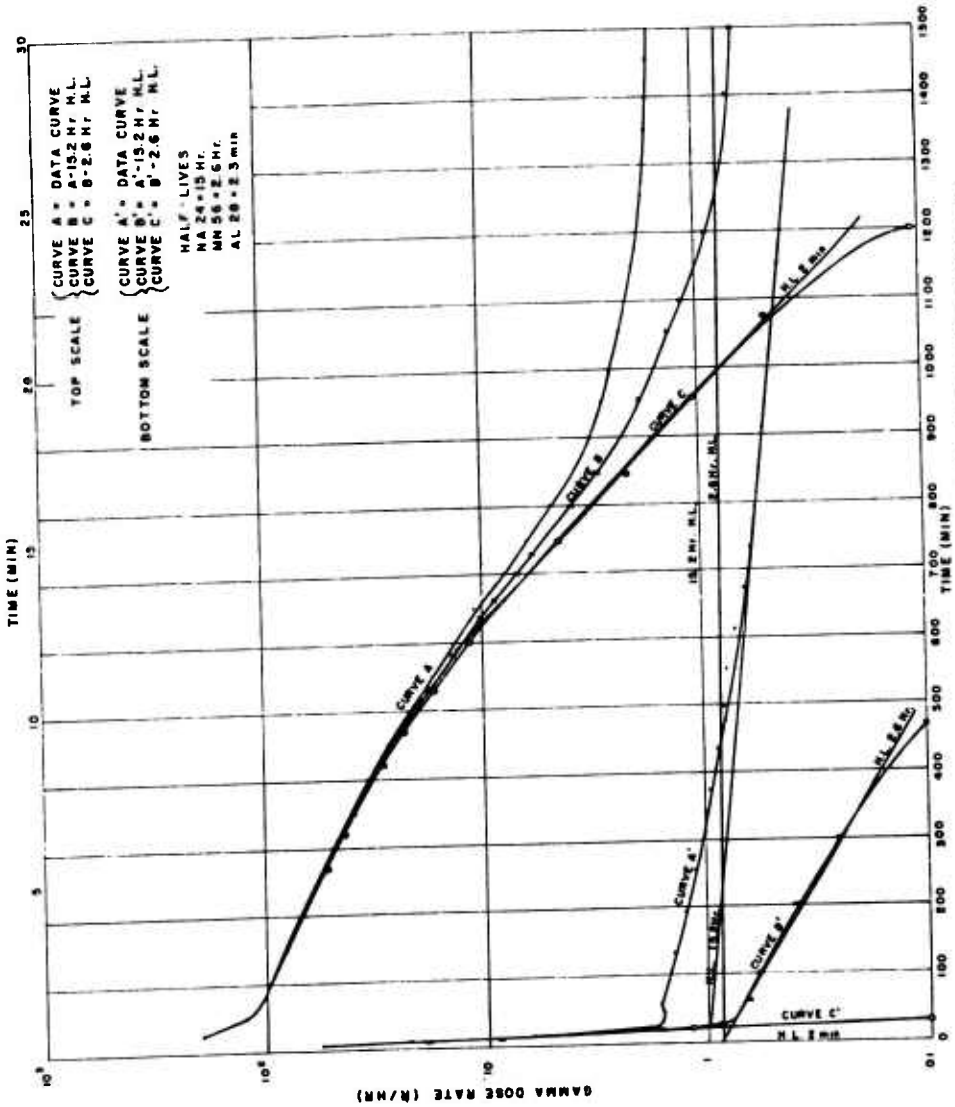

Figure 3.20 Intensity-versus-time curves, Shot Wasp', Ionization Chamber T, 437 yards, 215 degrees.

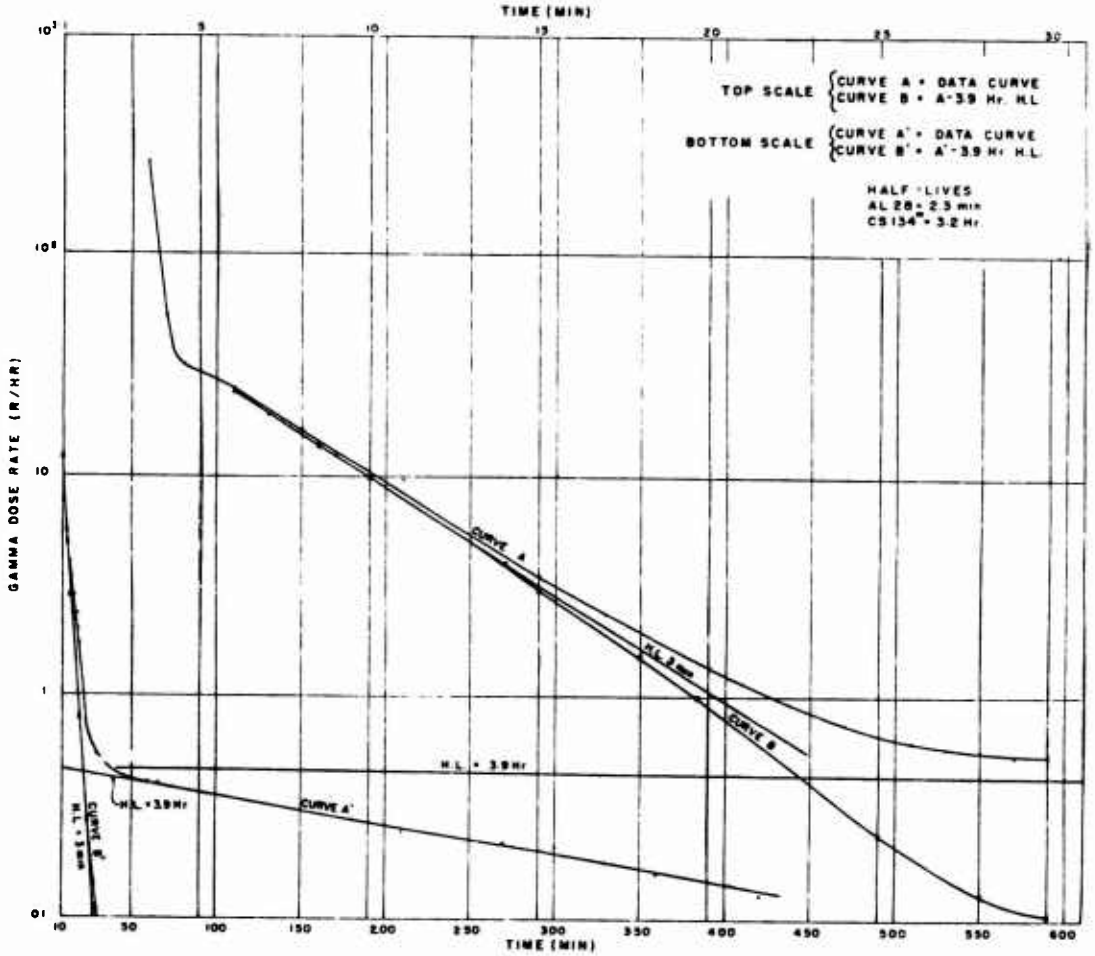

Figure 3.21 Intensity-versus-time curves, Shot Wasp, Ionization Chamber S, 642 yards, 95 degrees.

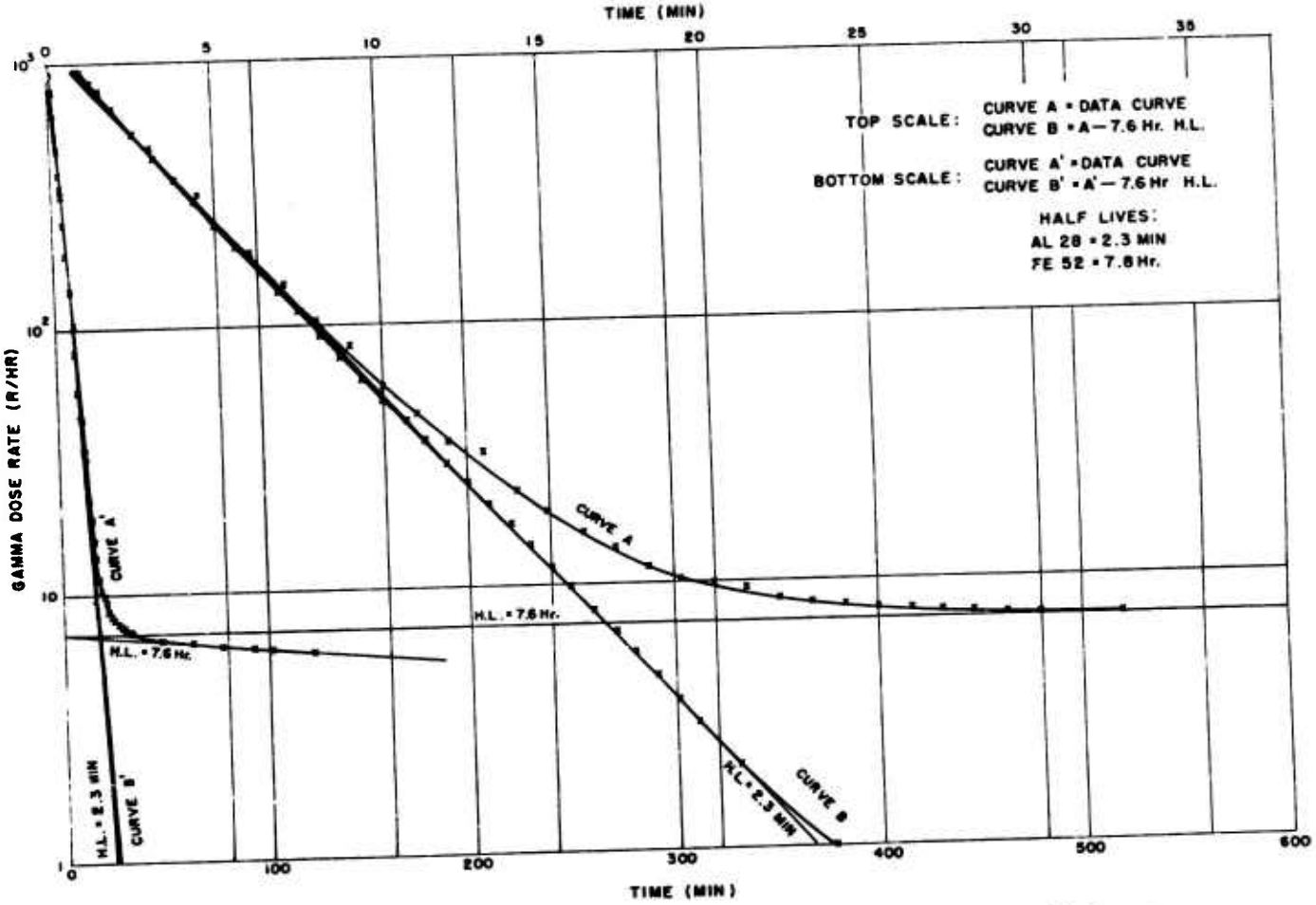

Figure 3.22 Intensity-versus-time curves, Shot Wasp', Scintillation Detector 3, 470 yards, 335 degrees.

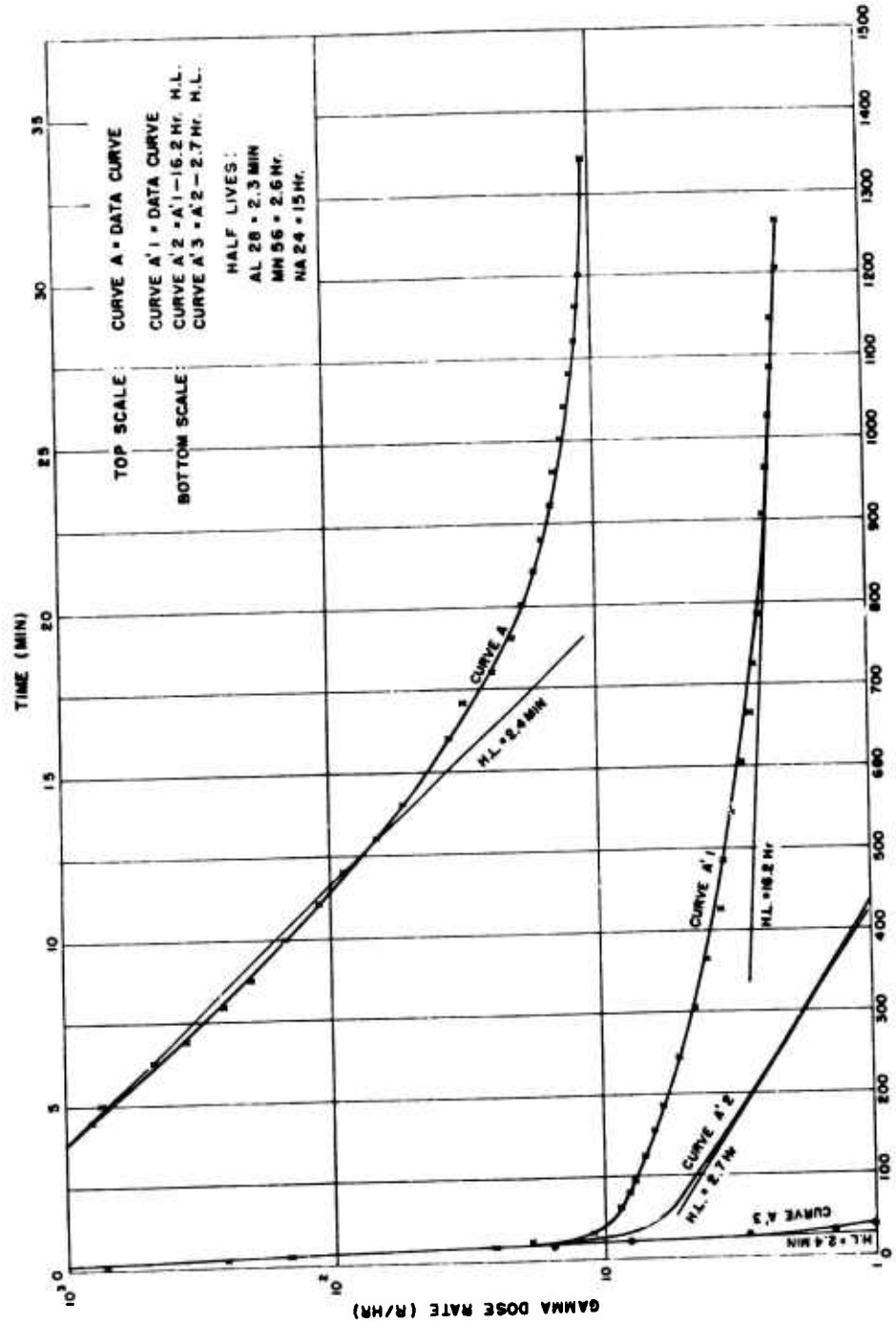

Figure 3.23 Intensity-versus-time curves, Shot Wasp', Scintillation Detector 13, 517 yards, 215 degrees.

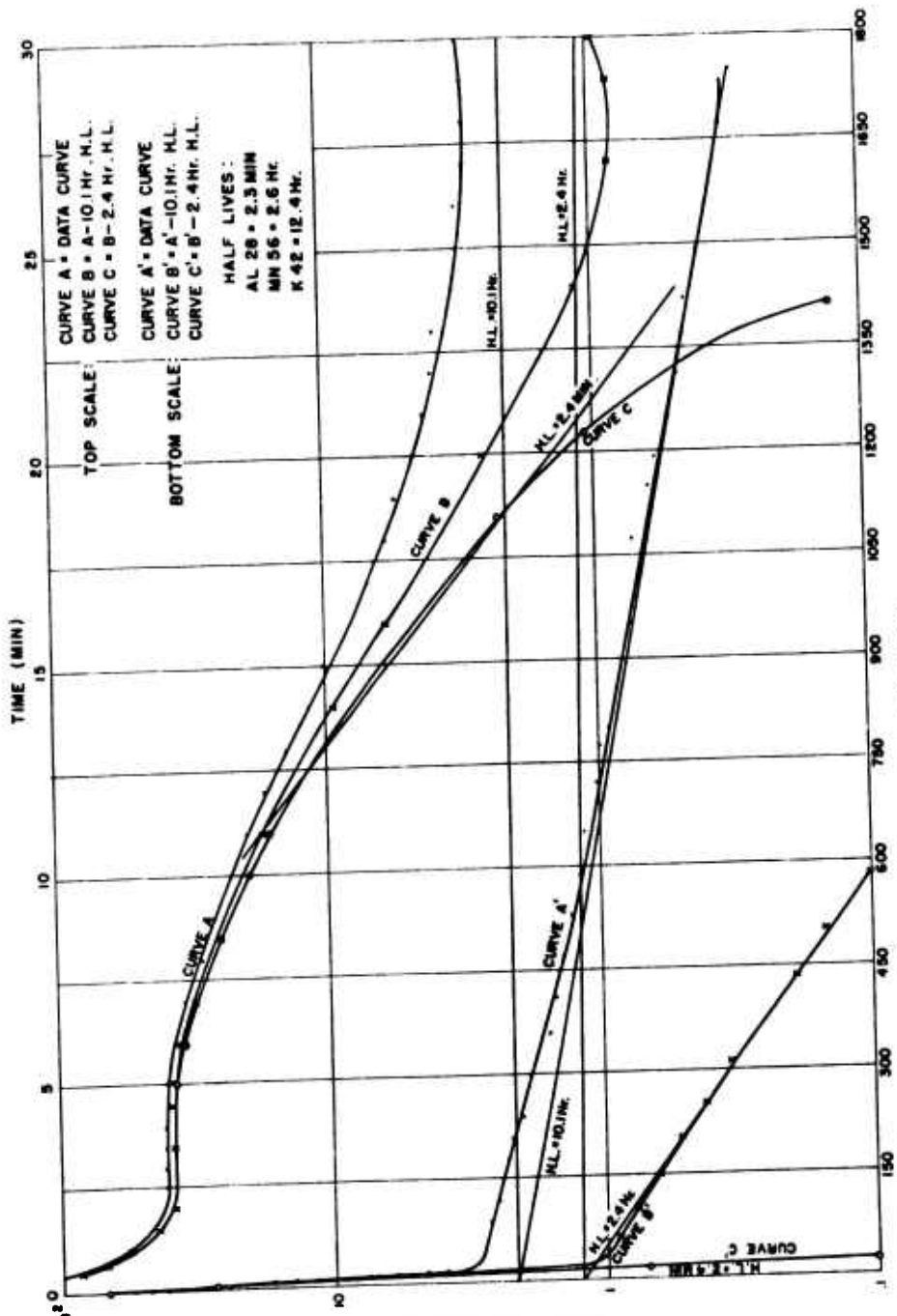

Figure 3.24 Intensity-versus-time curves, Shot Wasp', Ionization Chamber U, 517 yards, 95 degrees.

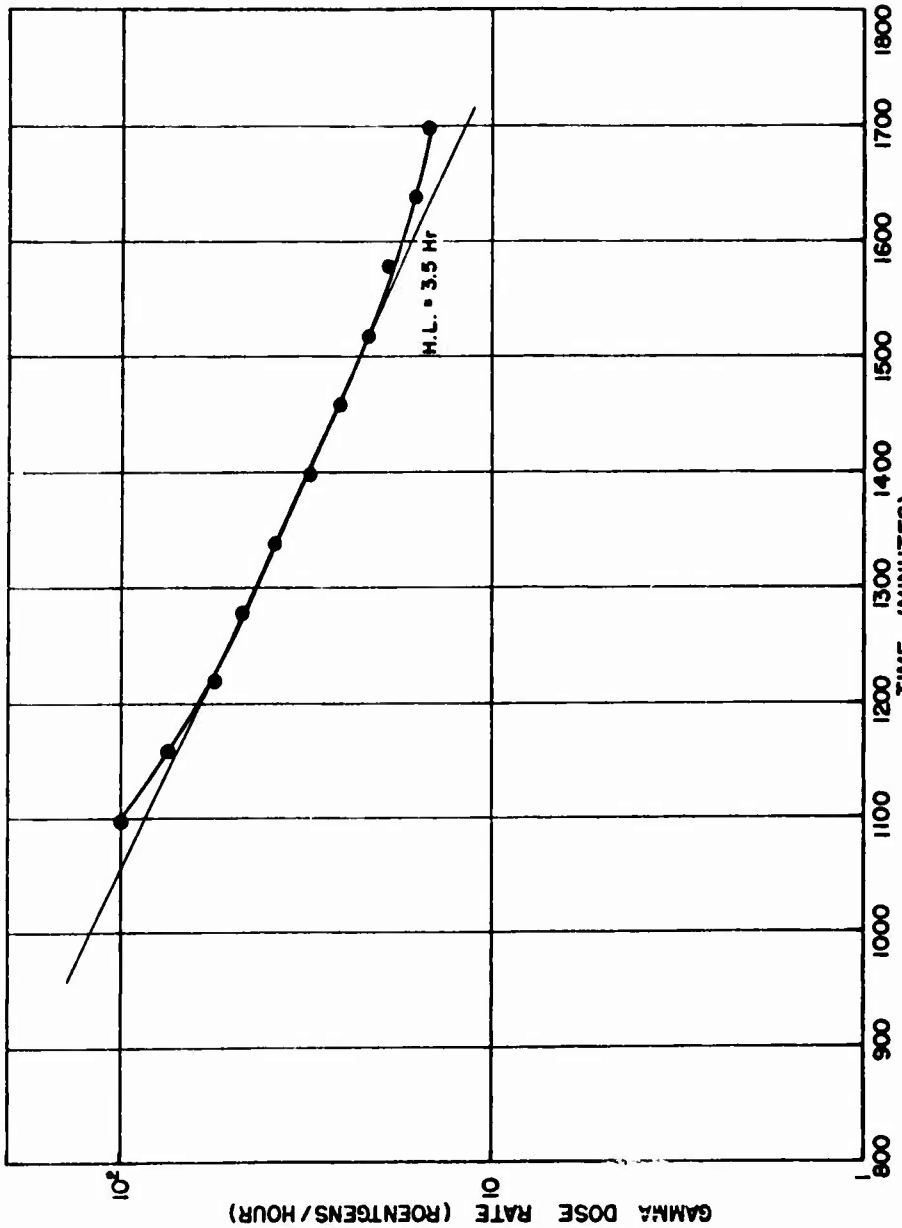

Figure 3.25 Intensity-versus-time curve, Shot Moth, Ionization Chamber P, 300 yards, 25 degrees.

TABLE 3.8 CALCULATION OF RELATIVE IMPORTANCE FACTOR FOR ISOTOPES IN NEVADA SOIL WHICH UNDERGO (n, γ) REACTIONS

Isotope	Isotopic Abundance by Weight	Isotopic Abundance	Isotopic Abundance	Activation Cross Section (σ)	Product Isotope	Product Half-Life	Transitions		$\Sigma E_\gamma \mu$ (f)	Relative Importance Factor (F)
							μ	E_γ		
	pct	gm/cm^3	atoms/cm^3	mb			pct	Mev	Mev	
Al^{27}	8.9	0.104	2.63×10^{21}	230	Al^{28}	2.27 min	100	1.78	1.78	1.345×10^{22}
Mn^{55}	0.078	0.00091	9.6×10^{18}	13,200	Mn^{56}	2.58 hr	20 30 100	2.06 1.71 0.822	1.75	8.25×10^{19}
Mg^{26}	1.602	0.0188	4.4×10^{20}	60	Mg^{27}	9.5 min	20 100	1.01 0.84	1.04	1.26×10^{20}
K^{41}	0.133	0.0154	2.6×10^{20}	1,190	K^{42}	12.4 hr	20	1.51	0.302	6.85×10^{18}
Na^{23}	0.67	0.0785	2.1×10^{20}	505	Na^{24}	15 hr	99.96 0.04 99.963	2.76 4.14 1.38	4.1	2.72×10^{19}
Ti^{50}	0.0069	0.00008075	9.7×10^{17}	200	Ti^{51}	5.8 min	100	0.32	0.32	1.93×10^{17}
Fe^{58}	0.00845	0.0000984	1.07×10^{19}	800	Fe^{59}	1,080 hr	50 50 50	0.20 1.30 1.10	1.30	1.35×10^{16}
S^{36}	0.0039	0.0000398	2.7×10^{18}	2.3	S^{37}	25.1 days	10 90	4.3 2.7	2.86	1.79×10^{14}
N^{15}	0.0036	0.0000421	1.4×10^{19}	100	N^{16}	7.4 sec	80	6.13	4.9	0.472
Cl^{37}	0.0185	0.00216	3.5×10^{19}	560	Cl^{38}	37.5 min	31 47	3.60 2.5	2.14	5.6×10^{19}

cylinder is a reasonable approximation to the shape of the blast shield as shown in Figure 3.26):

$$\phi = \frac{St}{2} [F(\alpha, \theta_1) + F(\alpha, \theta_2)] \qquad (3.3)$$

Where: ϕ = flux, photons/cm²-sec
S = specific activity, photons/cm³-sec
t = thickness of cylinder, cm
α = 0, for detector at center of cylinder
$\theta_2 = \theta_1 = \tan^{-1} h/2b$ for detector at center of cylinder
h = length of cylinder, cm
b = radius of cylinder, cm

Specifically: $\phi = St[F(0, \theta)]$

But: $F(0, \theta) = 0.0175\,\theta$ with θ expressed in degrees (Reference 19)

Therefore: $\phi = 0.0175\,St \tan^{-1} h/2b$

For the detector used: t = 0.419 cm
h = 23.17 cm
b = 2.8 cm
$\tan^{-1} h/2b$ = 76.25 degrees

Therefore: $\phi = (0.0175)(0.419)(76.25)\,S$
$= 0.5591\,S$

and $S = \frac{\phi}{0.5591}$

Since by definition a roentgen represents an absorption of 83.8 ergs of energy per gram of air, the flux of 1.78 Mev gamma rays required to give 1,000 r/hr is (Reference 20):

$$\phi = \frac{DE_f}{E_p} = \frac{(0.278)(3,352)}{2.85 \times 10^{-6}} = 3.27 \times 10^8 \text{ photons/cm}^2\text{-sec}$$

Where: D = dose rate = 10^3 r/hr = 0.278 r/sec
E_f = energy flux per roentgen

$$= \frac{83.8}{(\mu/\rho)_{air}} = \frac{83.8}{0.025} = 3,352 \text{ ergs/cm}^2$$

$(\mu/\rho)_{air}$ = mass absorption coefficient for air for 1.78 Mev gamma = 0.025 cm²/gm

E_p = energy per photon = 1.78 = 2.85×10^{-6} ergs/photon

Thus: $S = \frac{\phi}{0.5591} = \frac{3.27 \times 10^8}{0.5591}$

$= 5.84 \times 10^8$ photons/cm³-sec of aluminum shield

The density of soil is 1.17. Since aluminum is 8.9 percent of soil by weight, there are 0.104

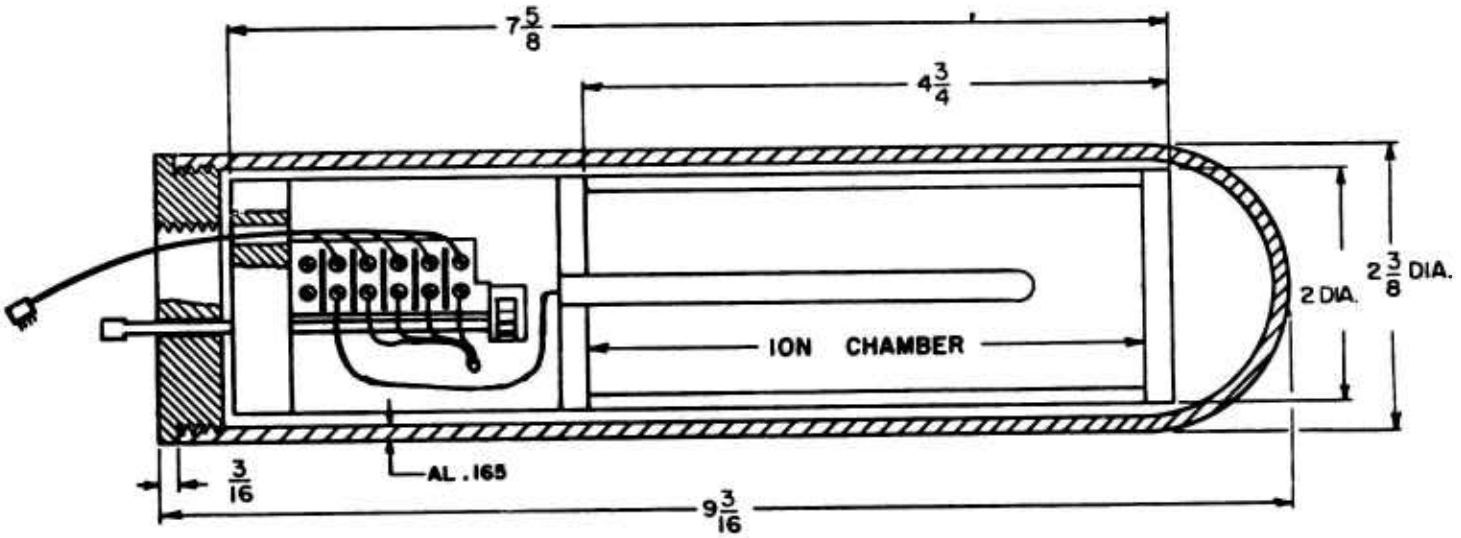

Figure 3.26 Detail of detector head with aluminum blast shield. (Weight of aluminum shield, 496 grams.)

gms of aluminum for each cubic centimeter of soil. The specific activity of soil is:

$$\frac{0.104}{2.7}\,(5.84 \times 10^{8}) = 2.25 \times 10^{7} \text{ photons/cm}^2\text{-sec}$$

To determine the gamma flux seen by the detector from the aluminum in the soil, the following expression may be used (Reference 21):

$$\phi = \frac{BS_A}{2}\,E_1(b_1) \tag{3.4}$$

Where: ϕ = flux, photons/cm^2-sec

B = build-up, taken as unity[1]

S_A = source strength, photons/cm^3-sec (same as specific activity of the soil in the present calculations)

$$E_1(b_1) = \int_{b_1}^{\infty} e^{-b}/b\, db \tag{3.5}$$

Where: $b = \mu t$

μ = linear absorption coefficient of air, cm^{-1}

t = the path length in air from the differential point source to detector, cm

$b_1 = \mu t_1$

t_1 = thickness of air slab (detector height above ground), cm

Equation 3.5 is a logarithmic integral, and is evaluated in Reference 22. For small values of b_1:

$$E_1(b_1) = \ln \frac{1}{\gamma b_1} \tag{3.6}$$

Where: $\gamma = 1.781072$ (Reference 22)

$t_1 = 91.4$ cm

$\mu = 5.78 \times 10^{-5}$ cm^{-1}

$b_1 = 91.4 \times 5.78 \times 10^{-5} = 5.28 \times 10^{-3}$

$$E_1(b_1) = \ln \frac{1}{1.78 \times 5.28 \times 10^{-3}} = \ln(106.4) = 4.66$$

The flux from the aluminum in the soil is:

$$\phi = \frac{2.25 \times 10^{7} \times 4.66}{2} = 0.524 \times 10^{8} \text{ photons/cm}^2\text{-sec}$$

The flux from the aluminum shield (1,000 r/hr of 1.78 Mev gammas) is:

$$\phi = 3.27 \times 10^{8} \text{ photons/cm}^2\text{-sec}$$

[1] It is to be noted that the build-up factor B in Equation 3.4 is itself a function b. Dr. W. S. McAfee of this laboratory has derived an integral form of Equation 3.4 for the case of single scattering applicable to the conditions of this experiment. It is found that the integral form of Equation 3.4 yields a value of ϕ which is only 20 percent greater than the result obtained by taking B equal to one.

Thus, the fraction of the total recorded dose rate coming from the soil is:

$$\frac{\text{Soil } \phi}{(\text{Shield} + \text{Soil})\,\phi} = \frac{0.524 \times 10^9}{(3.27 + 0.524)\ 10^9} = 0.138$$

A comparison between the observed neutron-induced fields from Shots Wasp and Wasp' at 1 hour and those predicted by TM 23-200, 1 June 1955 edition, is made in Table 3.9.

The predicted values are reasonably close to the observed values, although the prediction was based on high-neutron-yield devices. Reference 8 shows that the ratio of neutrons from Shot Wasp' to those of Shot Wasp was 7.06. The neutron ratio of Project 2.4 stations W-I to W'-I (approximately the same slant range) was 3.67, and when correction was made for distance (Reference 2), a ratio of 5.2 was obtained. Although stations were instrumented on Shots Moth and Tesla, only one instrument obtained data on Shot Moth and none obtained data on Shot Tesla. Shot

TABLE 3.9 PREDICTED AND OBSERVED INTENSITIES, SHOTS WASP AND WASP PRIME

Shot	Station	Slant Range	Intensity	
			Predicted	Observed
		yd	r/hr	r/hr
Wasp	W-I	500	3.6	1.65
Wasp	W-III	690	0.54	0.45
Wasp Prime	W'-I	527	7.1	6.1
Wasp Prime	W'-II	572	4.6	3.5
Wasp Prime	W'-III	572	4.6	2.5

Tesla's measured neutron flux (Reference 10) was 11.9 times as great as that of Shot Wasp. However, as no instruments functioned on Shot Tesla, an analysis based on neutron-flux strength and high-explosive configuration could not be made.

Chapter 4
CONCLUSIONS and RECOMMENDATIONS

4.1 CONCLUSIONS

4.1.1 Underground Burst. From the analysis of Shot Ess data, it is concluded that after 10 minutes the decay of activity is approximated by a function of the type:

$$D = At^{-1.2}$$

Where: D = dose rate
A = a constant based on distance and yield
t = time after detonation

The apparent rapid decay observed for the first few minutes after arrival of peak activity is attributed to movement of the radioactive air mass past the detector station. Because of the dynamic changes occurring in the radioactive source being detected at this time, the dose rate readings are not relatable to decay of the contaminant itself.

Faulty recorder-tape transports precluded a reasonable conclusion about arrival times. Nuclear detonation environment did change the response of the radiation detectors used on this test. Only a program to investigate the effects of devices on electronic components and detecting devices can solve this problem.

Because of the problems with instrumentation under field conditions, the absolute values of both the ordinates and abscissas in the dose-rate-versus-time measurements could not be determined too accurately.

4.1.2 Air Burst. The results show that the residual activity following air bursts is that induced in the elements of the soil. Furthermore, the relative importance factor based on soil analysis gives an accurate indication of the elements producing the radiation. In Nevada soil Al^{28}, Mn^{56}, and Na^{24} contribute most of the activity. No evidence of fallout was found.

4.2 RECOMMENDATIONS

4.2.1 Underground Burst. A repeat experiment with other instrumentation is recommended for better accuracy in dose-rate-versus-time measurements.

4.2.2 Air Burst. For more accurate measurements of induced activity, the instrumentation must be shielded from the neutron flux, or the induced activity in the components must be accounted for.

Appendix
SCINTILLATION and ION-CHAMBER DETECTORS

SCINTILLATION DETECTOR (Figure A.1)

The scintillation detector used a stilbene crystal mounted in a bakelite holder with a 0.6-cm wall thickness for electronic equilibrium. The light output of the crystal was measured by a 6199-type photomultiplier tube used in a feedback circuit that gave a log response to light and, hence, to radiation. The dynode voltage was obtained across the cathode resistor of the pentode control tube, used as a cathode follower.

The output of the photomultiplier tube was directly connected to the control grid of the pentode and, in operation, the output current of the photomultiplier tube anode was kept essentially constant by changing the dynode voltage. To reduce photomultiplier gain with increasing signal, the output signal was taken from the dynode voltage and varied as the log of the light input. Thus the dynode voltage was proportional to the log of the radiation level. A suitable portion of the dynode voltage was tapped off with a voltage divider, fed to a power amplifier, and then recorded on an Esterline-Angus, 0-to-1-ma recording milliammeter. Teledeltos, a dry-writing chart paper, was used instead of the conventional inking arrangement.

ION-CHAMBER DETECTOR (Figure A.2)

The ion-chamber instrument utilized the log-type response of an unsaturated ion chamber to provide a simple wide-range instrument. The electrometer circuit used a Victoreen high-meg resistor as the grid leak, and was connected as a cathode follower. The chamber voltage was obtained from a tap on the cathode resistor of the electrometer tube and was adjusted for 4 volts with no radiation. In addition, this connection provided a degree of positive feedback that tended to cancel the drop in chamber voltage caused by the drop across the high-meg resistor.

The output signal was then fed to the power amplifier and recorded on an Esterline-Angus, 0-to-1-ma recording milliammeter, converted to use Teledeltos.

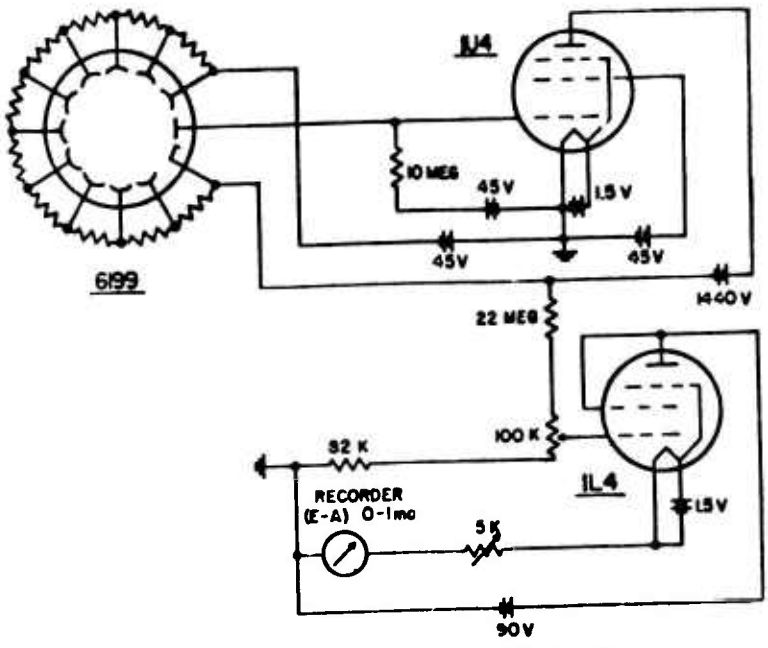

Figure A.1 Schematic diagram of scintillation detector.

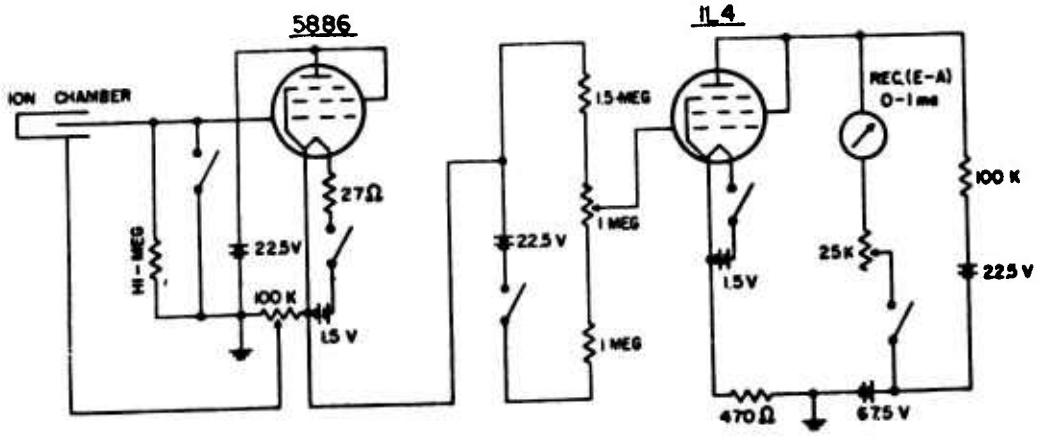

Figure A.2 Schematic diagram of ion-chamber detector.

REFERENCES

1. M. G. Schorr and E. S. Gilfillan; "Predicted Scaling of Radiological Effects to Operational Weapons"; Project 2.0, Operation Jangle, WT-391, 15 June 1952; Technical Operations, Inc., Arlington, Massachusetts; Secret Restricted Data.

2. "Capabilities of Atomic Weapons"; TM 23-200, November 1957; Armed Forces Special Weapons Project, Washington, D. C.; Confidential.

3. M. G. Schorr and E. S. Gilfillan; "Predicted Scaling of Radiological Effects to Operational Weapons"; Project 2.0, Operation Jangle, WT-391, page 2, 15 June 1952; Technical Operations Inc., Arlington, Massachusetts; Secret Restricted Data.

4. S. Glasstone; "The Effects of Nuclear Weapons"; 1957; U. S. Government Printing Office, Washington, D. C.; Unclassified.

5. K. Way and E. P. Wigner; "The Rate of Decay of Fission Products"; Physical Review, 1 June 1948, Vol. 73, No. 11, Page 1329; Clinton National Laboratories, Oak Ridge, Tennessee; Unclassified.

6. J. Orear and others; "Nuclear Physics"; Revised Edition, 1950; University of Chicago Press, Chicago, Illinois; Unclassified.

7. B. E. Watt; "Energy Spectrum of Neutrons from Thermal Fission of U^{235}"; Physical Review, Vol. 87, No. 6, 15 September 1952; Unclassified.

8. T. D. Hanscome and D. K. Willet; "Neutron Flux Measurements"; Project 2.2, Operation Teapot, WT-1116, 28 July 1958; U. S. Naval Research Laboratory, Washington, D. C.; Secret Restricted Data.

9. M. Cowan, Jr. and T. B. Cook, Jr.; "Residual Contamination from Nuclear Bursts"; SC-3466 (TR), 15 February 1955; Page 51, para. 4; Sandia Corporation, Albuquerque, New Mexico; Secret Restricted Data.

10. S. Glasstone; "Sourcebook on Atomic Energy"; 1950; D. Van Nostrand Company, New York, N. Y.; Unclassified.

11. G. L. Felt, and A. C. Graves; "Criteria for Future Continental Tests"; Report of Committee to Study Nevada Test Site, 2 February 1954; Los Alamos Scientific Laboratory, Los Alamos, New Mexico; Secret Restricted Data.

12. R. F. Johnson and others; "Neutron-Induced Radioactive Isotopes in Soils"; Project 2.3a, Operation Teapot, WT-1117, 7 August 1958; U. S. Naval Radiological Defense Laboratory, San Francisco, California; Secret Formerly Restricted Data.

13. M. J. Schumchyk and E. H. Bouton; "Fallout Studies"; Project 2.5.1, Operation Teapot, WT-1119, 23 July 1958; Chemical Warfare Laboratories, Army Chemical Center, Maryland; Confidential Formerly Restricted Data.

14. J. B. Graham and others; "Gamma Exposure versus Distance"; Project 2.1, Operation

Teapot, WT-1115, July 1957; U.S. Army Signal Research and Development Laboratory, Fort Monmouth, New Jersey; Secret Restricted Data.

15. P. W. Krey and others; "Soil Activation by Neutrons"; Project 2.1, Operation Plumbbob, ITR-1410, 6 December 1957; Chemical Warfare Laboratories, Army Chemical Center, Maryland; Secret Restricted Data.

16. "Handbook of Chemistry and Physics"; 38th Edition, 1956-1957; Chemical Rubber Publishing Company, Cleveland, Ohio; Unclassified.

17. S. Kinsman and others; "Radiological Health Handbook"; November 1954; U.S. Department of Health Education and Welfare; Robert A. Taft Sanitary Engineering Center, Cincinnati, Ohio; Unclassified.

18. J. G. Lewis and others; "Analysis of Radiation Sources"; Nucleonics, January 1954, Vol. 12, Page 40; McGraw-Hill Publishing Company, Inc., New York, N. Y.; Unclassified.

19. M. C. Atkins and others; "Design and Use of a 23,000-curie Cobalt-60 Facility"; Project 7360, WADC Technical Report 57-498, Chapter II, November 1957; Wright Air Development Center, Wright-Patterson Air Force Base, Ohio; Unclassified.

20. G. Hine and G. Brownell; "Radiation Dosimetry"; 1956; Page 12; Academic Press, New York, N. Y.; Unclassified.

21. T. Rockwell III; "Reactor Shielding Design Manual"; TID 7004, March 1956, Page 353; Naval Reactors Branch, Division of Reactor Development, Atomic Energy Commission, Oak Ridge, Tennessee; Unclassified.

22. F. Jahnke and F. Emde; "Tables of Functions"; Dover Publications, Inc., New York, N. Y.; Unclassified.